This document was prepared for the ETI by third parties under contract to the ETI. The ETI is making these documents and data available to the public to inform the debate on low carbon energy innovation and deployment.

Programme Area: Marine

Project: PerAWAT

Title: Tidalfarmer Interim Model Validation Report

Abstract:

Validation of the numerical models developed in TidalFarmer is essential in order to predict the expected energy yield with a quantifiable level of uncertainty. This will provide stakeholder confidence in the planning, investment and maintenance of a tidal array and will help accelerate growth of the tidal energy industry. The purpose of the interim report is to detail how PerAWAT data sets will be used to validate each model, the current results of model validation and uncertainty analysis. Further work that is required to have confidence in the model predictions is also discussed. Experimental measurements taken in the near wake region have been analysed to determine the wake width and maximum velocity deficit. This will form part of a parameterisation study in order to assess the capability and limitations the GH near wake model. It will be seen that the current data sets provide extensive information, but do not cover a sufficient number of rotor performance points such as Ct and ambient turbulence intensity. The GH flow field model is a solution to flow along a flat plate. Given that the seabed at tidal sites of interest is likely to be uneven, the GH flow model will be compared to a variety of experimental and numerical data sets for flow over varying bathymetry. The primary aim will be to assess the capability of the model to recover flow acceleration and deceleration.

Context:

The Performance Assessment of Wave and Tidal Array Systems (PerAWaT) project, launched in October 2009 with £8m of ETI investment. The project delivered validated, commercial software tools capable of significantly reducing the levels of uncertainty associated with predicting the energy yield of major wave and tidal stream energy arrays. It also produced information that will help reduce commercial risk of future large scale wave and tidal array developments.

GL Garrad Hassan

ETI Marine Programme Project
PerAWaT MA1003
WG3WP4 D18 TIDALFARMER INTERIM MODEL VALIDATION REPORT

Client	**Energy Technologies Institute**
Contact	Geraldine Newton-Cross
Document No	104329/BR/18
Issue	Draft
Classification	Not to be disclosed other than in line with the terms of the Technology Contract
Date	28th Sep 2012
Author:	S Parkinson, J Giles, M Thomson
Checked by:	Rob Rawlinson-Smith
Approved by:	Unapproved

Garrad Hassan & Partners Ltd

St Vincent's Works, Silverthorne Lane, Bristol BS2 0QD, UK Tel: +44 (0)117 972 9900, Registered in England 1878456

IMPORTANT NOTICE AND DISCLAIMER

1. This report ("Report") is prepared and issued by Garrad Hassan & Partners Ltd ("GH" or "Garrad Hassan") for the sole use of the client named on its title page (the "Client") on whose instructions it has been prepared, and who has entered into a written agreement directly with Garrad Hassan. Garrad Hassan's liability to the Client is set out in that agreement. Garrad Hassan shall have no liability to third parties (being persons other than the Client) in connection with this Report or for any use whatsoever by third parties of this Report unless the subject of a written agreement between Garrad Hassan and such third party. The Report may only be reproduced and circulated in accordance with the Document Classification and associated conditions stipulated or referred to in this Report and/or in Garrad Hassan's written agreement with the Client. No part of this Report may be disclosed in any public offering memorandum, prospectus or stock exchange listing, circular or announcement without the express written consent of Garrad Hassan. A Document Classification permitting the Client to redistribute this Report shall not thereby imply that Garrad Hassan has any liability to any recipient other than the Client.
2. This report has been produced from information relating to dates and periods referred to in this report. The report does not imply that any information is not subject to change.

KEY TO DOCUMENT CLASSIFICATION

Strictly Confidential	:	For disclosure only to named individuals within the Client's organisation.
Private and Confidential	:	For disclosure only to individuals directly concerned with the subject matter of the Report within the Client's organisation.
Commercial in Confidence	:	Not to be disclosed outside the Client's organisation
GH only	:	Not to be disclosed to non GH staff
Client's Discretion	:	Distribution for information only at the discretion of the Client (subject to the above Important Notice and Disclaimer).
Published	:	Available for information only to the general public (subject to the above Important Notice and Disclaimer and Disclaimer).

REVISION HISTORY

Issue	Issue date	Summary
Draft	20/08/12	GH internal draft
Draft	31/08/12	Version following Rob Rawlinson-Smith comments
Draft	02/09/12	Submission of D18 with interim flow field modelling work
Final	28/09/12	Re-submission of D18 following comments from ETI.

CONTENTS

LIST OF FIGURES

LIST OF TABLES

EXECUTIVE SUMMARY

Validation of the numerical models developed in TidalFarmer is essential in order to predict the expected energy yield with a quantifiable level of uncertainty. This will provide stakeholder confidence in the planning, investment and maintenance of a tidal array and will help accelerate growth of the tidal energy industry.

Given the delays experienced in the PerAWaT sub-projects, at present there is insufficient data to allow a full validation of the GH blockage, near wake, far wake and flow field models. The purpose of the interim report is to detail how the data sets will be used to validate each model, the current results of model validation and uncertainty analysis. Further work that is required to have confidence in the model predictions is also discussed.

The blockage model will be compared to both analytical models and experimental data obtained through the PerAWaT project. This will provide preliminary evidence that the model is reproducing the effects of wake blockage as expected. Further model validation is required in order to compare the model for a variety of different lateral, vertical and area blockage ratios.

Experimental measurements taken in the near wake region have been analysed to determine the wake width and maximum velocity deficit. This will form part of a parameterisation study in order to assess the capability and limitations the GH near wake model. It will be seen that the current data sets provide extensive information, but do not cover a sufficient number of rotor performance points such as Ct and ambient turbulence intensity.

The 2-d and 3-d far wake model will be compared to experimental readings of the flow field interaction with multiple devices. This will investigate the ability to recreate the merging of multiple wakes generated by devices operating as an array. These test cases only focus on a particular range of Ct values and ambient turbulence intensities. Therefore, further experimental evidence is required to have confidence in the velocity deficit predictions.

The GH flow field model is a solution to flow along a flat plate. Given that the seabed at tidal sites of interest is likely to be uneven, the GH flow model will be compared to a variety of experimental and numerical data sets for flow over varying bathymetry. The primary aim will be to assess the capability of the model to recover flow acceleration and deceleration.

SUMMARY OF NOTATION

Channel characteristics

A	Cross-sectional area (m^2)
b	Width of channel (Diameters)
D_H	Hydraulic radius of the channel (m)
Fr	Froude number (channel)
h	Channel height (Diameters)
r	Radial distance (m)
z	Vertical height measured from the sea bed or channel floor (m)

Turbine characteristics

C_p	Power coefficient
Cp_b	Power coefficient of the rotor in a boundless flow
C_t	Thrust coefficient
Ct_b	Thrust coefficient of the rotor in a boundless flow
D	Rotor diameter (m)
hh	Turbine hub height (Diameters)
$Re_{turbine}$	Reynolds number across the rotor

Flow Field

a	Axial induction factor
B	Blockage ratio
B_l	Lateral blockage ratio
B_v	Vertical blockage ratio
E	Specific energy (m^2/s^2)
f	Body forces (per unit volume) acting on the fluid (N/m^3)
g	Gravitational acceleration (m/s^2)
J_0	Bessel function
M	Momentum (Ns)
m	Strength of the source
p	Pressure (N/m^2)
q	Flow rate (m^3/s)
R	Radius of streamtube (m)
S	Area of the streamtube (m^2)
s_t	Equivalent 2-D turbine diameter (m)
s_0	Width of streamtube upstream (m)
s_2	Width of streamtube downstream (m)
u	Axial velocity component (m/s)
v	Lateral velocity component (m/s)
w	Vertical velocity component (m/s)
U_0	Mean free stream flow speed (m/s)
U_i	Incident flow speed on rotor (m/s)
I_{amb}	Ambient turbulence intensity
α	Fractional reduction in velocity downstream in the wake (m/s)
β	Fractional reduction in velocity at the rotor (m/s)
Φ	Velocity potential (m^2/s)
κ	Drag coefficient

ρ	Density (kg/m^3)
τ	Fractional increase in flow speed (m/s)
1-d	one dimension (typically in the x-direction)
2-d	two dimensions
3-d	three dimensions

Near Wake

Û	Normalised velocity deficit
μx	Mean x-position for Gaussian fit to measured data
μy	Mean y-position for Gaussian fit to measured data
σx	Standard deviation in x-direction for Gaussian fit to measured data
σy	Standard deviation in y-direction for Gaussian fit to measured data
E	Mean error between measured and GH model predictions

Far Wake

F_{k1}	Eddy-viscosity mixing parameter
S_0	Start of the near wake

A general glossary on tidal energy terms was provided as part of WG0 D2 – "Glossary of PerAWaT terms". This is a working document which will be revised as the project progresses.

1 INTRODUCTION

1.1 Scope of this document

This document constitutes an interim report of the GH blockage, near wake, far wake and flow field models as part of the eighteenth (D18) deliverable of working group 3, work package 4 (WG3WP4) of the PerAWAT (Performance Assessment of Wave and Tidal Arrays) project commissioned and funded by the Energy Technologies Institute (ETI). Garrad Hassan (GH) is the sole contributor to this work package. This document describes the methodology for validation of the GH blockage, near wake, far wake and flow field models and discusses the results of comparisons with measured data from model-scale experiments as well as numerical simulations.

1.2 Purpose of this document

The purpose of WG3WP4 is to develop, validate and document an engineering tool that allows a rapid assessment of the energy yield potential of a tidal turbine array on non-specialist hardware. The specific objective of WG3 WP4 D18 is to both document and provide a technical justification for the use of the existing GH blockage, near wake, far wake and flow field models within the suite of models that make up the engineering tool: TidalFarmer.

1.3 Specific tasks associated with WG3 WP4 D18

WG3WP4 D18 comprises the following aspects:

- A description of the GH blockage, near wake, far wake and flow field model and assumptions.
- Evaluation of each of each GH model against available experimental and numerical data sets.
- An estimate of the model uncertainty when comparing measurements against GH model predictions.
- Assessment of parameters space for which model is valid, i.e. operating Ct value, etc.
- Discussion of validity of the GH model assumptions.
- Next steps summary of the work that is required in order to ascertain the aggregated accuracy of the GH energy extraction tool.

1.4 WG3 WP4 D18 acceptance criteria

The acceptance criteria as stated in schedule five of the PerAWAT technology contract is as follows:

D18: TidalFarmer interim model validation report:

- Description of validation methodology for the blockage model.
- Assessment of blockage model performance via the analysis of the boundless rotor characteristics, the device scale experiment data (RPM, power and thrust) and the model results.
- Quantification of the uncertainties of the GH blockage model
- Discussion of the overall validity, sensitivities and limitations of the GH blockage model

- Description of validation methodology for the near wake model.
- Assessment of near wake model performance via the comparison of the device scale experiment data with the GH near wake models – particularly, the near wake form (in terms of deficit and turbulence intensity).
- Analysis of the effect of varying the shear profiles on the near wake form in a variety of ambient flow conditions (waves and seabed generated turbulence intensities).
- Assessment of the effect of including the flow field data from the ReDAPT project on near wake model performance.
- Quantification of the uncertainties of the GH near wake model.
- Discussion of the overall validity, sensitivities and limitation of the GH near wake model.

- Description of the validation methodology for the flow field model.
- Assessment of model performance via the comparison of the detailed 2-d Telemac model against the rationalised flow model with the basin scale data form ReDAPT.
- Validation of depth profile models (data from ReDAPT).
- Quantification of the uncertainties of the GH flow field model.
- Discussion of the overall validity, sensitivities and limitations of the GH flow field model.

- Description of validation methodology for the far wake model.
- Assessment of model performance via comparison of the device scale experiment data and the GH far wake models, particularly wake deficit and added turbulence intensity, conditions and wave generated turbulence.
- Assessment of the impact of large scale eddies on wake recovery.
- Assessment of wake interaction modelling – via comparison with experimental data.
- Quantification of the uncertainties of the GH far wake model.
- Discussion of the overall validity, sensitivities and limitations of the GH far wake model.

2 PERAWAT DATA

For viable commercial energy generation, tidal turbines will need to be deployed in large arrays where infrastructure economies of scale can be realised. Typical commercial-sized farms are expected to be of the same rated power order of magnitude as offshore wind farms i.e. 100s of MWs (MacKay, 2008). The implication of this and the nature of bi-directional tidal flows means it is likely that the spacing between turbines will be minimised, within practical installation and site specific seabed conditions constraints.

The operation of an array of tidal stream turbines gives rise to issues such as reduced energy yield and increased loading on turbine blades. To this end, GH have developed and documented several models (Thomson *et al*, 2010b, c, 2011a, b, c) that describe the physical process of energy extraction from an array of tidal stream turbines. These are the blockage model, near wake model, far wake model, and flow field model.

The GH modelling philosophy is to provide practical engineering solutions to real world problems using modelling techniques that can be implemented and run using readily available computational power (i.e. desk top or laptop personal computers). To be of value to the Tidal Energy industry, the GH models must be shown to produce good results in comparison to experimental, numerical and analytical models and therefore provide stakeholders with confidence in the numerical algorithms developed by GH and on the energy yield estimates produced by TidalFarmer.

Below the various data sets available to GH in order to validate the blockage, near wake, far wake, and flow field models are summarised. The discussion will focus on what information can be derived from the data concerning the respective models we wish to validate. In the field of fluid mechanics, there exists three disciplines all of which are inter-related. These are: analytical solutions, computational fluid dynamics and physical experimentation. None of these disciplines can stand alone when attempting to understand a physical problem and validate models. Consequently, each field has been utilised through the PerAWaT project.

2.1 Model validation

Experiments undertaken through the PerAWaT project are discussed in this section. The details of interest include: which model the experiment relates to, what physical quantities will be varied, and when the data will become available.

2.1.1 WG4 WP1 Device scale experimentation

The $1/30^{th}$ scale physical experiments (Buvat, 2012) performed at Chatou will provide information about the near wake structure and far wake of a bare horizontal axis turbine, when operating in a variety of ambient turbulence intensity, flow speeds and wave climates. Readings were taken at lateral and vertical transacts at multiple positions downstream in order to obtain detailed measurement of the near awake dynamics. This information is invaluable when validating both the near wake and blockage models at a range of thrust values imparted on the flow. In addition, the tests cover a range of turbulence intensities which will improve confidence in the different input parameters available in the GH models.

At the time of writing, the report is due for submission at the end of September 2012. In this report, we will present some of the processed data from the `detailed' test case. A comparison with the GH models will be made in D19.

2.1.2 WG4 WP2 Array scale experimentation

Investigations of array interactions at farm scale were undertaken at the University of Manchester (Thomson *et al*, 2011a). These studies allow wake merging between multiple devices to be investigated. Readings were generally taken at lateral and vertical transacts just downstream of the devices at 2D to measure the near wake and then further downstream to measure wake mixing.

The wake measurements taken at 2D just downstream of the devices will be used to measure the wake width and velocity deficit. This data can be used to formulate a parameterisation of the near wake. In addition, the readings further downstream can be used to compare against results from the far wake model. Finally, the lateral spacings of the devices were varied for different arrangements such that blockage effects due to adjacent devices could be analysed.

The preliminary results from these comparisons will be presented later in this report.

2.1.3 WG4 WP3 Ducted single device experiments

At this stage in the PerAWaT project there is limited experimental data for ducted rotors. The objective of the ducted experiments performed under WG4 WP3 (Stallard, 2012) is to fill this gap in knowledge. This experiment will lead to data that can be used to validate the far wake model and also provide near wake data for a ducted machine. The turbine used in WG4 WP2 will be placed in the flume used to obtain the measurements in WG4 WP1. The primary parameters that will be investigated will be the position of the device in the shear layer and a number of thrust operating points.

As the time of writing the experiments have not yet begun. The present schedule suggests that all measurements will be taken by 31st November 2012. Therefore, a comparison to this data set will have to be performed in D19.

2.1.4 WG4 WP4 Regional scale experimentation

The objective of the 1/300th scale experiments carried out at the coastal research facility in HR Wallingford was to understand the effect of energy extraction on regional scale flow (Wickham & Way, 2012). The devices themselves were represented using emulators (porous discs). A variety of different basin and device layouts were considered including headlands and different sizes of arrays.

The devices impart thrust on the flow and allow us to compare against the blockage model to measure the impact of multiple devices on the local flow field.

2.1.5 ReDAPT

Rotor performance and loading data from the ReDAPT (Reliable Data Acquisition Platform for Tidal) project will also be utilised when it becomes available. At the time of writing the exact extent of the data that will become available from the ReDAPT project is yet to be confirmed, however, Table 1 outlines the data that is expected to become available and which may be used in the validation of TidalFarmer.

Table 1: Data from the ReDAPT project that can be used for model validation.

		Method of binning	Flow field model	Device model	Blockage model	Near wake model	far wake model
ReDAPT site measurements	Device power output and inflow data	x			x		
ReDAPT site measurements	Measurement of the site turbulence		x			x	x
ReDAPT site measurements	far wake recovery using long range sensor and seabed mounted ADCP						x
ReDAPT simulation data	Validated CFD model of near wake					x	x
ReDAPT simulation data	Validation of Tidal Bladed to confirm inflow and Ct,Cp relationship			x	x		
ReDAPT simulation data	Flow field model results		x				

2.2 Model verification

Here is a list of the numerical work that will be undertaken and the information that will be obtained through these investigations.

2.2.1 WG3 WP1 Single device numerical investigation

As part of the PerAWaT programme, sophisticated CFD models of rotors have been developed (McIntosh, 2011). These models can be used to investigate flow and geometry conditions which are not feasible in experimental facilities. At the time of writing, the results for WG3 WP1 D4 are only just becoming available.

The device modelled in WG3 WP1 D4 is based on the EDF 1/30th scale rotor used in WG4 WP1. The performance characteristics of the EDF rotor, as designed, have been replicated using the UoO embedded blade element momentum (BEM) model and a blade resolved algorithm. The model will utilise a volume of fluid algorithm to investigate the impact of the free-surface on energy extraction and performance of the rotor.

Numerical modelling in WG3 WP1 will investigate the effect of carrying the position of the turbine in the water column. The simulations will also test blockage, yaw and different shear profiles. In later deliverables the inclusion of wave effects will also be included.

The preliminary processed data will be presented and discussed in D18. However, as of yet a comparison to the data has not yet been formed with any of the GH models.

2.2.2 WG3 WP3 Telemac regional scale numerical experiments

EDF will develop their Telemac code to model energy extraction due to tidal stream turbines in WG3 WP3. This will then be compared to TidalFarmer so that aggregate uncertainties through the blockage and wake models can be understood. At the time of writing the EDF simulations for the `baseflow' have been performed (Martin *et al*, 2012). These simulations over an entire tidal cycle for three separate regions – the Pentland Firth, Paimpol-Brehat and Alderney have been performed. The objective of the later deliverable, D3, is to perform Telemac simulations that incorporate tidal stream turbines. Once these Telemac results become available, a cross-verification study with the energy extraction model in WG4 WP3 can be undertaken.

It is expected that the model simulations will be available by the 31st March 2013 in time for inclusion in report D19.

2.2.3 WG3 WP5 Numerical investigation of fundamental device concepts

The second numerical package that models single devices has been undertaken by the University of Edinburgh (Gretton, 2011). The objective of this work package is to model two different fundamental design concepts - a high solidity (open centre turbine) and low solidity (bare horizontal axis turbine) device.

These investigations will include examining different blockage ratios and the effects of turbulence intensity in the near wake region. Through this project, a parameterisation of the near wake will be realised and relationships on important parameters, such as rotor operating thrust coefficient and environmental conditions such as turbulence intensity, will be identified. This will inform the near wake model developed by GH.

The results of a parameterisation study of the near wake will be made available by 31st November 2012.

2.3 Analytic models

The use of analytic models that simplify the physics of a particular problem are also a source for comparison. For a simplified geometry and flow these models can provide meaningful results that are in good agreement with experimental measurements. Given the accuracy and low computational cost, these models also provide a source of cross-verification.

One such example is the work by Whelan (2009). This demonstrates the suitability of using 1-d corrected actuator disc theory for a highly blocked rotor comparing rotor thrust. This model will be used as a source for comparison with the blockage model in section 3.

3 BLOCKAGE MODEL

Traditionally a blockage correction was applied to measured wind tunnel data, so that the results from blocked flow (by the wind tunnel sidewalls) could be extrapolated to an unblocked flow (Wood & Harris, 1920). In the GH 3-d blockage model we invert this process, so that from the unblocked flow we may calculate the operating parameters due to flow blockage.

A turbine can be considered to be similar to a bluff-body at certain operating states (despite being effectively porous) because it has a significant wake flow. This situation can give rise to both wake and solid-body blockage. However, the axial length of a rotor is insignificant relative to its diameter and therefore its solid-body blockage will be minimal. Thus blockage effects caused by turbines are a direct result of wake blockage.

In a bounded domain, the effect of wake blockage will be to cause fluid to accelerate around the device (Thomson *et al*, 2010a). The introduction of other features around a tidal turbine, i.e. flows induced by other hydraulic structures or surfaces, will cause the rotor streamtube to deform from the axisymmetric shape shown in Figure 3-1. Changes in the streamtube cross-sectional area will change the performance and loading experienced by the rotor compared to the unbounded flow (Thomson, 2004).

The areas for commercial scale deployment of tidal arrays are typically where the water depth is between 20 – 100 metres. The desire to maximise energy capture means that the swept area of the tidal turbine will be at a practical maximum resulting in a non-dimensional depth of 1.5-5D. At these smaller depths there is likely to be a certain amount of flow blockage generated between the seabed and the free surface. These effects can be referred to as “vertical blockage” and defined by a “vertical blockage ratio” (turbine diameter/flow depth). Marine Current Turbine’s SeaGen turbine has a lateral spacing of 1.5D between the twin rotor centres (i.e. a gap of 0.5D). Thus the expected range for lateral spacings between adjacent devices could also be between 1.5D -5D. These effects can be referred to as “lateral blockage” and defined by a “lateral blockage ratio” (turbine diameter or lateral array width/channel width). Decoupling of vertical and lateral blockage effects will be important, particularly given the prospects of development in very shallow and wide resources such as the Severn Estuary (Giles, 2010).

Various studies have been conducted into the effects of blockage on turbines and bluff-bodies (Maskell, 1963), and developed to consider the free-surface, e.g. Scott (1976), Bai (1979), Durgun & Kafali (1991), Whelan (2009). The majority of early work only considered the area blockage effects and did not characterise the decoupled effects of vertical and lateral blockage.

Many first generation sites are likely to involve high vertical blockage but relatively low lateral blockage; hence these effects do require independent investigation. As mentioned earlier, the presence of bounding surfaces acts to re-direct the vertical and lateral components of the flow into the stream-wise direction, causing an overall increase in the flow through the swept area of the turbine. This leads to:

- increased torque or rotor speed (depending on the rotor control strategy),
- increased loading experienced by the turbine,
- potentially, increased power capture
- and, an altered flow field around the rotor

In combination, vertical and lateral bounding increase the potential blockage to a level which could have an appreciable effect on turbine performance. Thus it is considered important to quantify these effects. Combined vertical and lateral blockage can be measured by the "area blockage ratio" (turbine area/channel cross-sectional area).

The last point impacts on wake recovery and expansion. As the flow velocity in the bypass region around the turbine (and hence the wake) will be increased due to the restriction of bounding surfaces the resulting wake flow field, when compared with the same rotor operating in an unbounded flow, will be different. This in turn will have an impact on the rate of wake mixing and recovery. Hence when evaluating array performance and inter-array flow effects both the change in rotor performance and the alteration to the local flow field will need to be evaluated.

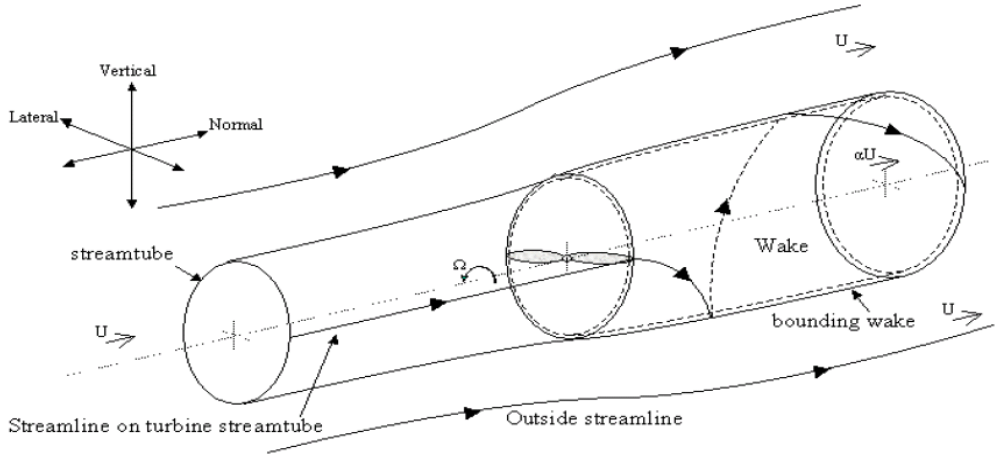

Figure 3-1: The near flow field in and around a rotor in an unbounded flow

3.1 General description of GH blockage model

The GH blockage model uses potential flow theory to model the deviation in the flow around a turbine because of blockage effects. This model is based on a multi-pole method where sources in a potential flow recreate the effects of the bounding surfaces and adjacent turbines (Thomson *et al,* 2010). The source strength is determined via an iterative procedure where a resistance coefficient is fixed using actuator disc theory. An algorithm is then implemented to determine the value of the source strength of each turbine in turn.

- Steady flow – For the analysis of performance change, the flow speed is constant. This assumes that the frequency of tidal flow is sufficiently small such that at any point in time the flow can be assumed to be quasi-steady.
- Inviscid – The high Reynolds flow regime implies that away from solid wall boundaries, viscous forces will be small, and that changes to performance will not be affected by viscosity.
- Irrotational – The assumption that the flow is irrotational implies that viscosity, and therefore turbulence is neglected. This is an idealisation of a high Reynolds number flow and produces suitable modelling results, one instance being potential flow solvers used in the Aerospace industry. However, by neglecting shear we are assuming the turbine is not located in a boundary layer. In addition, it is assumed that very little rotation is imparted into the flow by the wake streamtube. A correction for this is provided via linear momentum analysis.
- The pressure driven expansion of the streamtube can be represented by a simple source term and characterised by the boundless Ct.
- The non-slip condition is not modelled, as it is assumed that the mean flow over the rotor is uniform, leading to a uniform change in flow outside of the streamtube.
- The expected operational Froude numbers are low enough to ignore local surface disturbances.
- Rotor resistance coefficient is independent of blockage.

3.2 Validation methodology

The approach taken to evaluate the validity and associated uncertainties of the GH blockage model is discussed in the following sections. The purpose of the blockage model is to correct for blockage effects that are linked to bounding surfaces. A good measure of how blocked a channel is when considering the deployment of tidal stream turbines is not only the overall blockage ratio B but also the lateral B_l and vertical blockage B_v ratios.

To fully validate the blockage model, a comparison needs to be performed with data sets that have a wide variety of different (and realistic) blockage ratios. In the following section we will look at how this will be achieved by comparing to both the numerical, experimental and analytical results available to us throughout the PerAWaT project.

3.2.1 Analytical model comparison

The current focus will be to examine blockage effects at different blockage ratios, including lateral, vertical and area. As discussed in the methodology report, analytical models which can evaluate a blockage correction can be used to partly verify the GH potential model. The use of analytical models, as described in Section 3.4, provides a first approximation to assessing the impact of boundary surfaces upon the momentum extraction process.

Three analytical models are used here. The first is the classic boundless actuator disc approach (Burton *et al*, 2011). The second and third apply linear momentum theory to a 1-d tunnel and a 1-d channel as described in Whelan, *et al* (2009).

Using analytical models of a rotor, the effect of blockage upon the performance coefficients Cp and Ct can be compared. The value of Cp and Ct depend upon the operating point of the rotor, i.e. how much energy it is extracting and the common parameter used to describe the amount of momentum extraction is the axial induction factor *a*. Plots of Cp and Ct verse the axial induction factor for

different analytical models of blockage are examined in Section 3.4. The effect of blockage ratio and Froude number on the analytical solutions is also investigated using a range of values corresponding to 'typical' and 'extreme' conditions. The analytical models have been coded within Matlab for a multi-parameter analysis.

The analytical model solutions are limited to 1-d analysis and hence there is a need for slightly more sophisticated models. When comparing the solutions from the GH 3-d Potential model, the 2-d actuator disc tunnel model and the 1-d actuator disc model channel equivalent rotor areas must be used to maintain the same blockage ratio.

The potential flow model is also compared to the analytical models for different blockage ratios at the same rotor operating point, i.e. Cp, Ct vs Br.

The use of an actuator disc model also provides further valuable data for comparison with both the Potential flow model and the analytical solutions. However, actuator disc theory assumes perfect energy extraction. In reality rotor blades do not behave as actuator discs and the axial induction factor varies depending on many parameters including the blade geometry and both the incident flow speed and the rotor speed. The non-dimensional parameter used to characterise a real rotor's performance characteristics (i.e. Cp & Ct) is called the Tip-Speed-Ratio (TSR). And hence to compare the effect of blockage upon a real rotor comparisons must be made in the context of the variations in Cp & Ct vs TSR. To be able to fully understand the impact of blockage on real rotors we first need to know the rotor characteristics for boundless flow.

3.2.2 Experimental studies

Table 9 summarises the data sets available for model validation. From this data, a range of lateral, vertical and area blockage ratios will be examined. This range will allow us to assess the capabilities of the GH blockage model for a variety of different blockage ratios. A summary of this range is presented in Figure 3-2, Figure 3-3, and Figure 3-4. We can see that there is a reasonable spread of data covering different blockage ratios to validate the blockage model against. In particular, for lateral blockage we have a good range, however for area blockage we are missing data between 10 and 20 %. This will in some part be remedied by the numerical observations from WG3 WP1 where numerical simulations will examine a blockage ratio of around 10 %. In addition, for vertical blockage we are missing experimental data below 40 %. The experiments for the ducted rotor in WG4 WP3 will give data with a low vertical blockage ratio. It is noted that we do not want to consider flume data with over B>40 % blockage because this is more akin to a tidal fence which is not what we wish to model.

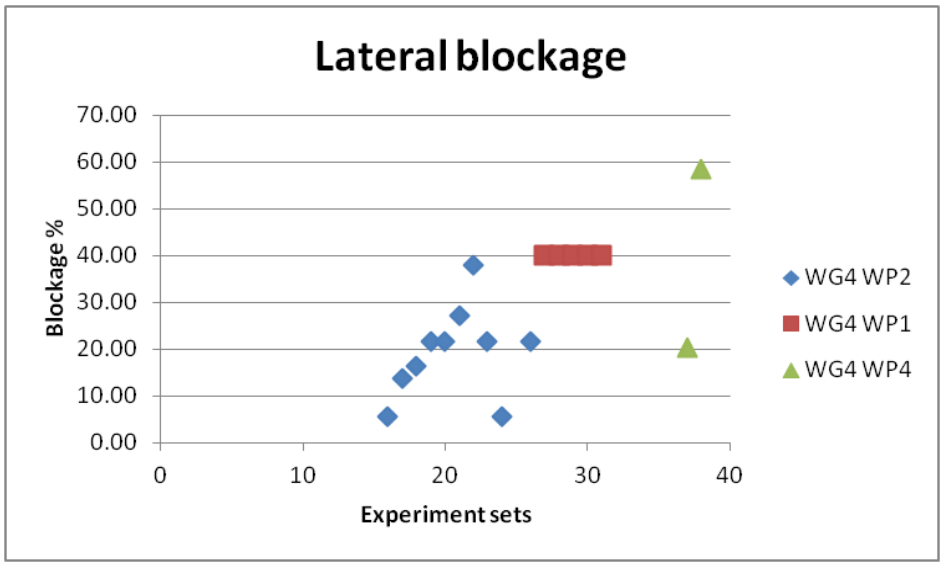

Figure 3-2: Spread of existing PerAWaT experimental data investigating lateral blockage.

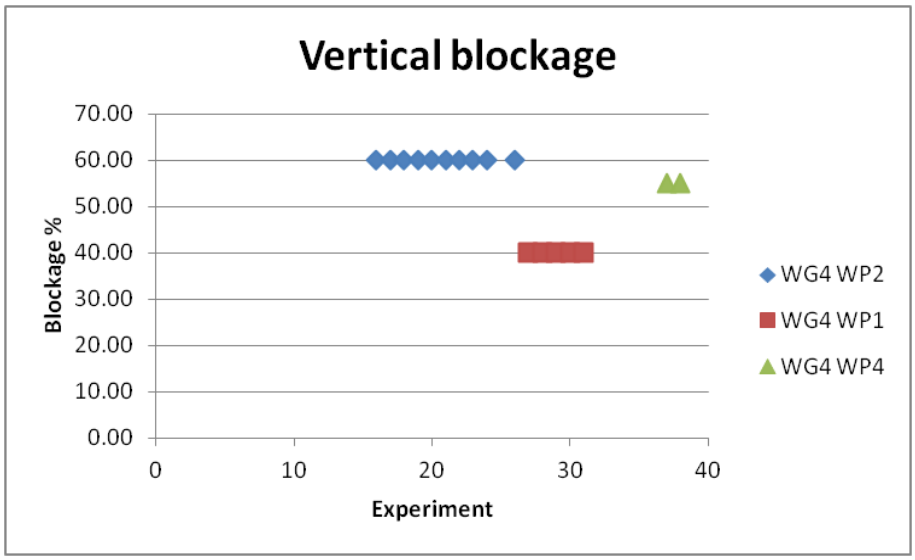

Figure 3-3: Spread of existing PerAWaT experimental data investigating vertical blockage.

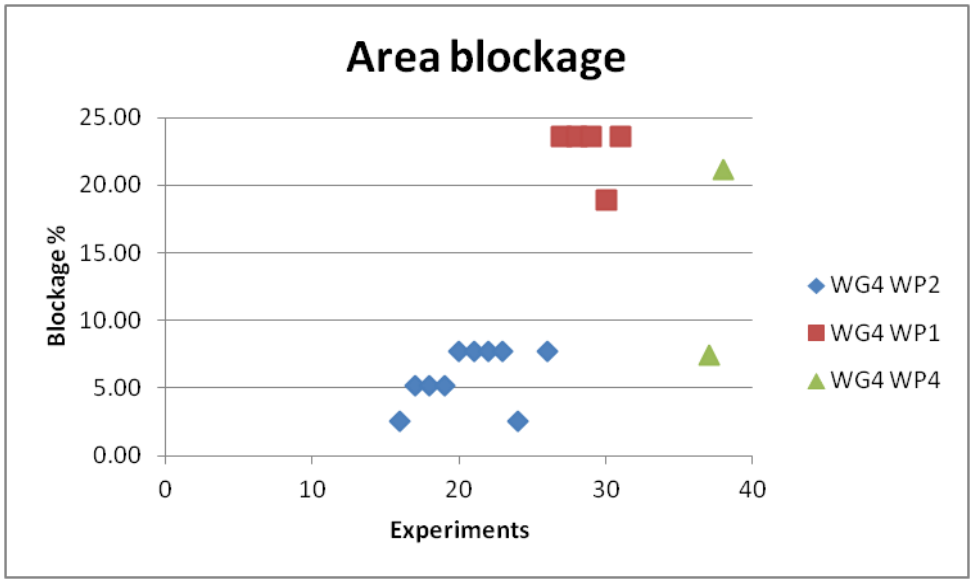

Figure 3-4: Spread of PerAWaT experimental data investigating the area blockage.

The spread of data affords a considerable source of comparison for the GH blockage model in order to assess limitations and uncertainty. In addition, the blockage ratio parameter space will be increased through numerical simulations providing further confidence in the model.

3.3 Model verification

Here we present the results of comparisons between analytic model solutions (referred to as the Boundless solution– standard actuator disc mode, Tunnel solution – adapted actuator disc to account

for four bounding surfaces, Channel solution – accounting for a free surface in the actuator model) and the GH blockage model (referred to as the Potential solution).

Figure 3-5 shows the variation in Cp and Ct with axial induction factor for the three analytical models at two different blockage ratios and two Froude numbers.

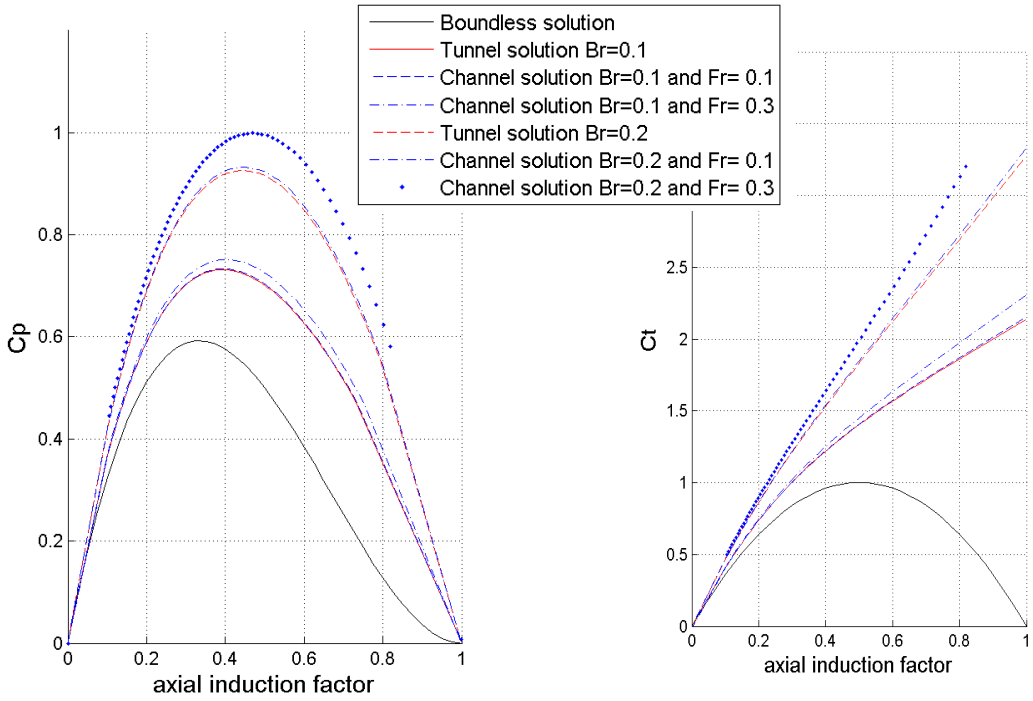

Figure 3-5: Analytical model results (Cp.Ct vs axial induction factor)

Blockage ratios of up to 20 % are considered on the basis that this is a practical limit for deployment of tidal turbines when considering lateral spacing and depth. The tunnel solution represents the zero Froude number condition and the channel solution is evaluated for a Froude number for two values: 0.1 and 0.3. The higher value provides a maximum (assuming a 3 m/s current at 40 metres depth). The lower is a more typical value. As can be seen the impact on the change in Cp and Ct is large and non-linear, but in the most severe cases the tunnel solution only varies from the channel solution by less than 1%.

For a feasible blockage ratio of 10% the peak Cp values are significantly greater than the boundless prediction. However, there are two points to note. First, these results relate to a 1-d system and second, the solutions presented do not account for any non-physical solutions. Actuator disc theory for the boundless case is limited to the range of axial induction factors from 0-0.5; a value greater than 0.5 represents wake flow reversal which cannot occur physically (Burton *et al*, 2011). The parameter used to indicate the limit to the axial induction factor is alpha (as defined in Section 2.4. 1 of Thomson & McCowen (2010a)). The left plot in Figure 3-6 shows Cp value against alpha, where as the right figure plots Cp against the axial induction factor. It can be seen that for the higher blockage ratios Cp does not peak for positive values of alpha. Alpha equal to zero corresponds to no wake flow (referred to as the propeller brake state for a boundless rotor), and hence alpha < 0 is physically not possible. To avoid reaching the state where wake flow stops real rotors tend to operate at values of alpha above 0.2.

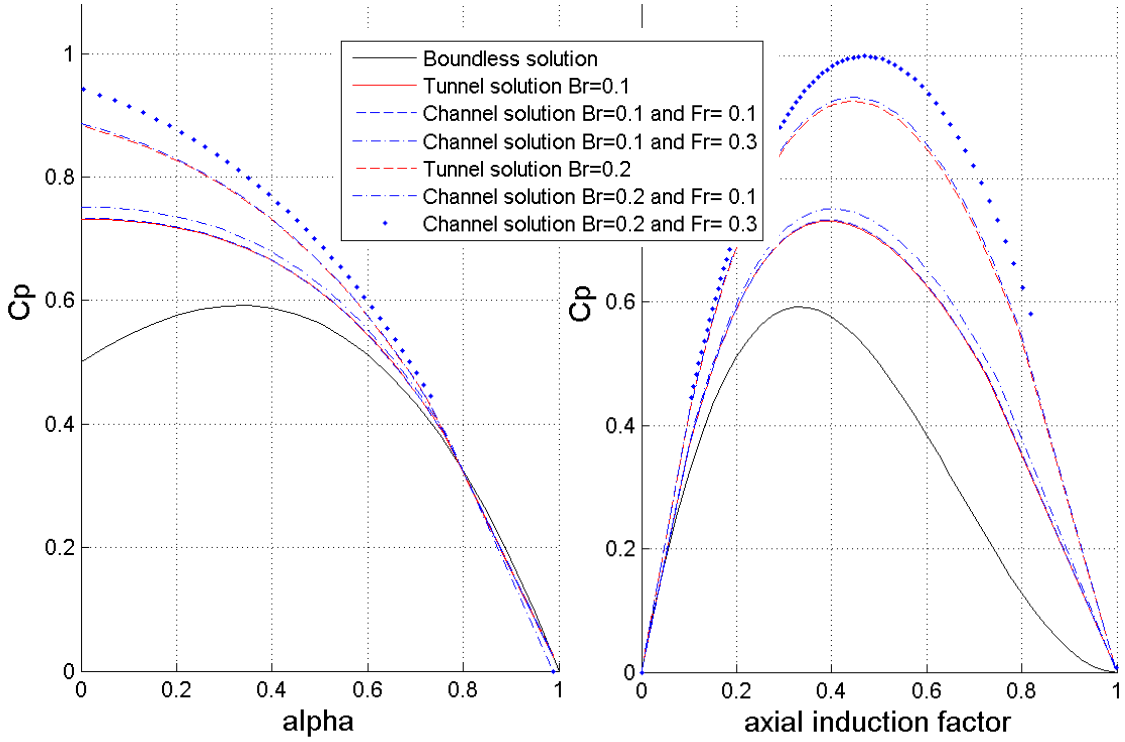

Figure 3-6 Analytical model results (Cp vs alpha and Cp vs axial induction factor)

The figure below includes the results of the GH Blockage model. It can be seen in the left plot how the potential model solution compares well with the boundless case and reasonably well with the two selected blockage ratios. The right plot shows the solution of the potential model when a correction factor to account for the errors introduced by the use of numerical methods is introduced. The numerical error arise from using the solutions of the flow field where the streamtube is not fully expanded. Note that the further work is required to improve the model to reduce the numerical errors.

Figure 3-8 plots the same data as in the right hand plot in Figure 3-9 but as Ct vs Cp. It can be seen that the general effect of blockage is to increase both Cp and Ct. In the region where real rotors are likely to operate (Ct=0.5-0.8) the models agree reasonably well.

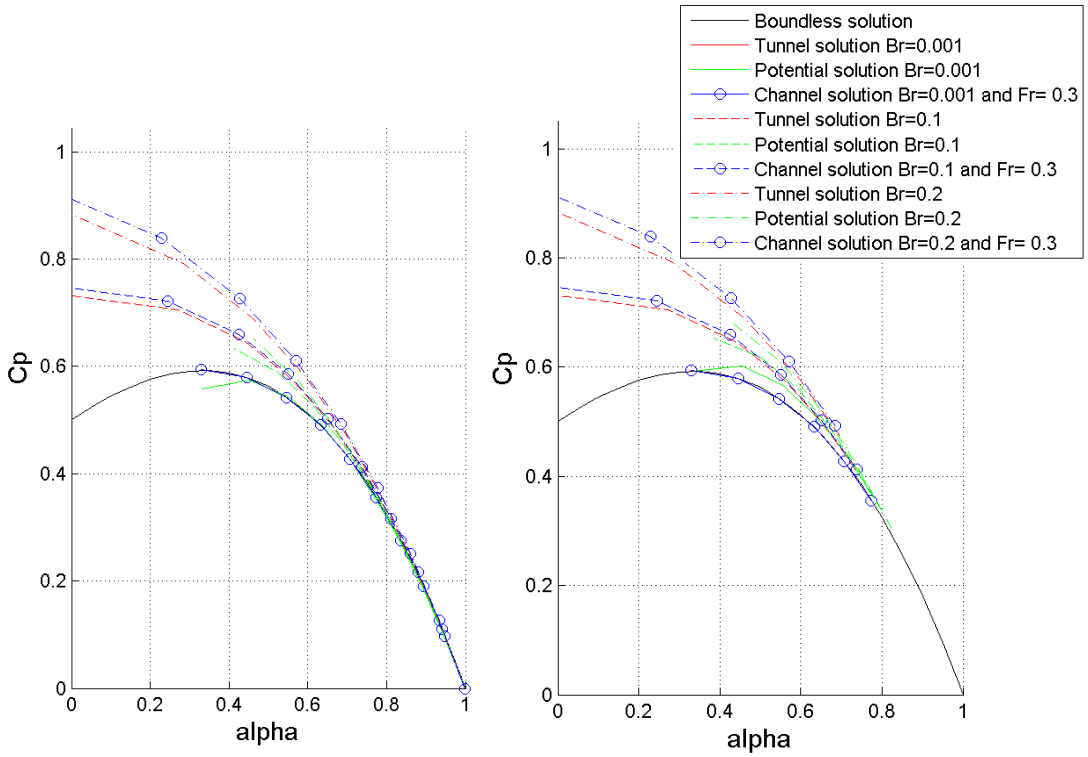

Figure 3-7: Analytical model comparison (Cp vs alpha) (left: without model correction, right: with model correction)

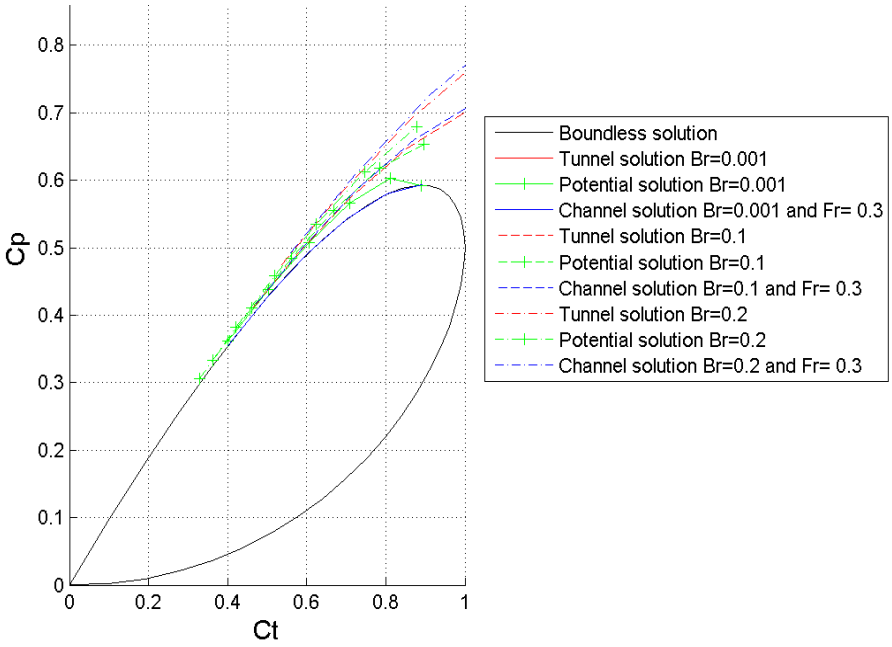

Figure 3-8: Analytical model comparison (Ct vs Cp)

The above plots have shown how the relationship between Cp, Ct and alpha (the fractional wake flow coefficient) vary with increasing blockage ratio and Froude number. However, these relationships do not provide sufficient information to compare a set of operating points for a blocked and unblocked condition. To compare the impact of blockage for a single operating point an assumption about the operating point needs to be considered. To do this it has been assumed that the pressure drop across the rotor remains constant. The figure below shows how the Cp and Ct vary with blockage ratio for the analytical and potential flow model.

The GH Blockage model compares well with the analytical models for the lower blockage ratios, but the correlation deteriorates for the higher blockage ratios. As stated previously, realistic blockage ratios are not likely to exceed 20%, and in this region the GH blockage model compares reasonably well although the agreement deteriorates as the blockage ratio increases.

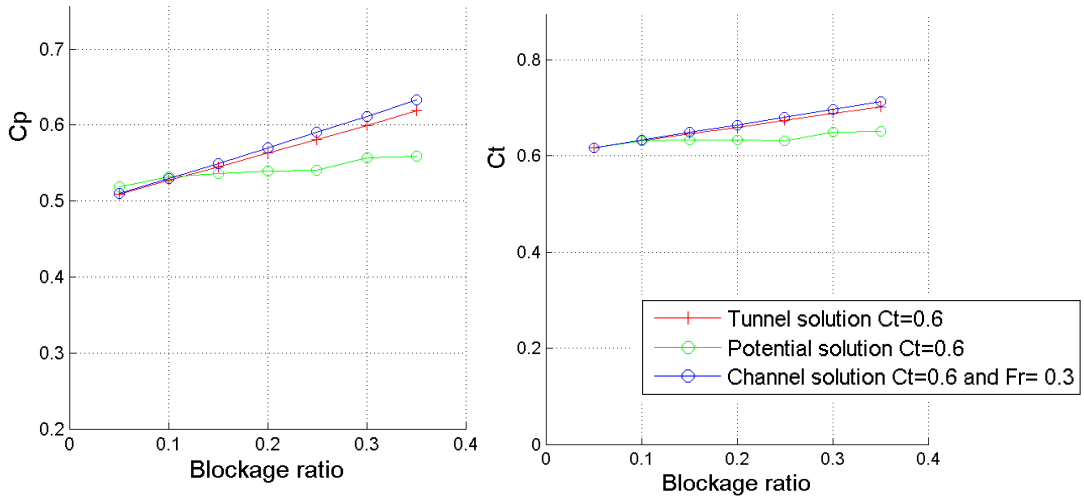

Figure 3-9: Analytical model comparison (Cp vs Blockage ratio)

3.4 Model validation

For non-ideal i.e. non-actuator disc rotors the effects of losses must be considered. As mentioned in Section 3.4 the parameters used to characterise real rotors are the Cp, Ct vs TSR curves. Hence to demonstrate the impact of blockage on real rotors Cp, Ct vs TSRs curves are examined.

3.4.1 Single rotor performance – EDF rotor

The figure below shows the measured Cp & Ct vs TSR for the as EDF rotor (full description of the rotor and tests can be found in WG4WP1 deliverables). To establish the impact of flume blockage upon the performance of the rotor channel analysis corrections have been applied (i.e. the equivalent boundless rotor performance has been calculated from the measured data. These corrected plots are also shown in the figure below. It can be seen that the effect of blockage increases both Ct and Cp and it changes the TSR value for the peak Cp and Ct operating points.

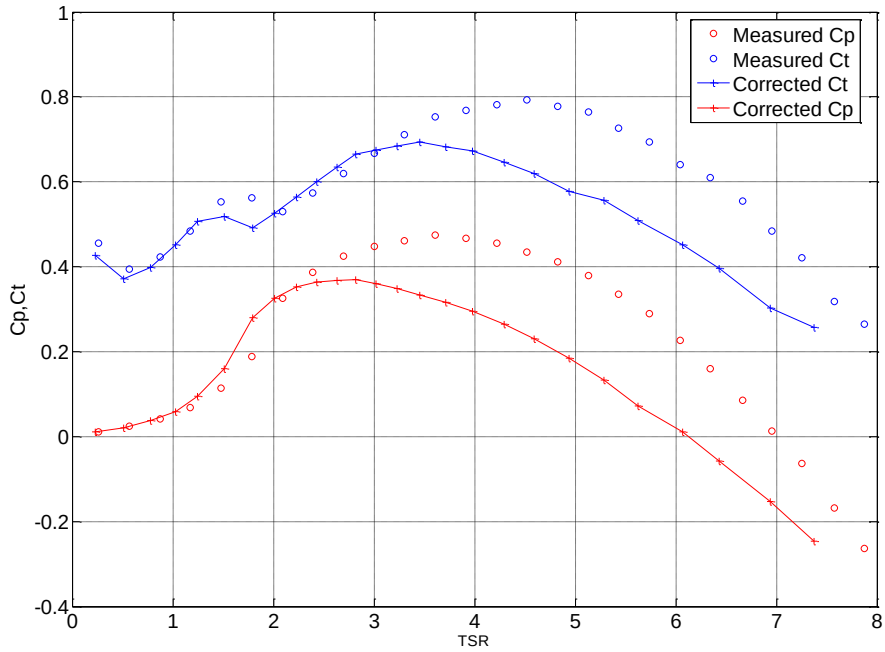

Figure 3-10: Cp & Ct vs TSR for the EDF rotor (with blockage correction applied)

To establish the validity of the channel model the corrected measurement values can be compared to the boundless predictions of Cp and Ct vs TSR constructed from Tidal Bladed. However, during the initial analysis it became clear that some geometric discrepancies occurred during the building of the EDF rotor. The impact of the discrepancies results in quite different operating characteristics as is seen in Figure 3-11 (solid vs dashed lines). The main different is the change in Ct at the higher TSRs. Figure 3-12 shows the results of numerical simulations undertaken by UoO (which account for the flume boundaries) and again the large effect the geometric discrepancies have on the predicted rotor performance is clear. However, it is also apparent that the measured data is different to the predicted data. The reason for the difference is not entirely clear, however, it is expected than it is a combination of factors from measurement error, uncertainties around the actual blade configuration, and also real blockage phenomena especially around the higher TSR values. Other research (Whelan 2009) has shown that the channel model is valid especially for similar lateral and vertical flume dimensions. Hence a reasonable amount of confidence is given to the channel model correction method.

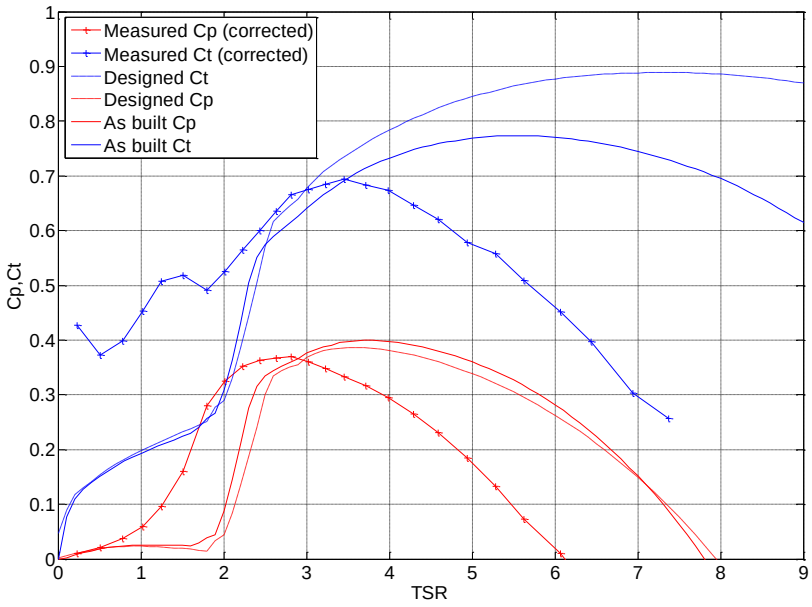

Figure 3-11: Cp & Ct vs TSR for the EDF rotor – measured (with blockage correction applied), designed(- - -) and as built (------).

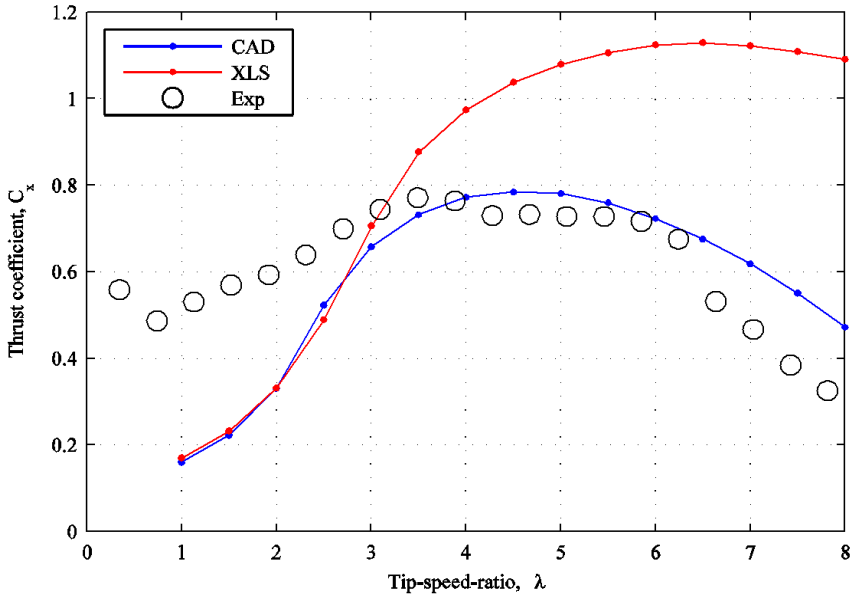

Figure 3-12: Comparison of UoO Ct predictions for different rotor geometries (note CAD refers to the as built blade geometry and XLS refers to the design geometry)

To provide some comparison between the channel and potential model the measured and corrected boundless prediction of the EDF rotor has been used as a baseline. The figure below shows how the potential model under predicts the effect of blockage around the peaks. It is expected that this deficit

can be address via model correction. However, more experimental data (physical or numerical) is required before a suitable correction can be developed.

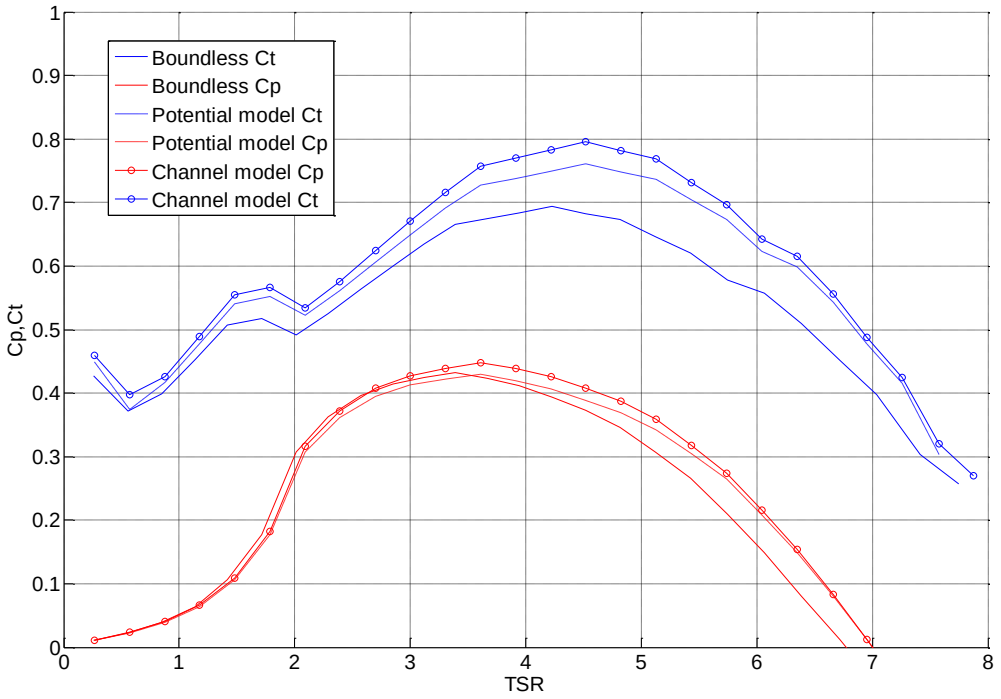

Figure 3-13: Cp & Ct vs TSR for the EDF rotor – measured (with blockage correction applied), designed and as built

3.4.2 Single rotor performance – UoM rotor

As part of the WG4WP2 several scale model tests have been performed. These tests were performed at 1/70th scale and the flow was fully turbulent (Thomson *et al*, 2011a). The scale rotors used within the UoM flume have enabled comparison of the boundless BEM prediction with that of the measurements. Error! Reference source not found. shows a single rotor's performance characteristics of Cp, Ct vs SR. The comparison is reasonable, with the Potential model predicting a greater increase in Ct due to blockage than the equivalent analytical model. This would be expected as the analytical models cannot incorporate the asymmetry of the experimental set-up. Compared to the measured data the Potential model is marginally under predicting the thrust. However, as shown by the grey bands the level of uncertainty around the rotor prediction is high and hence this could account for the difference.

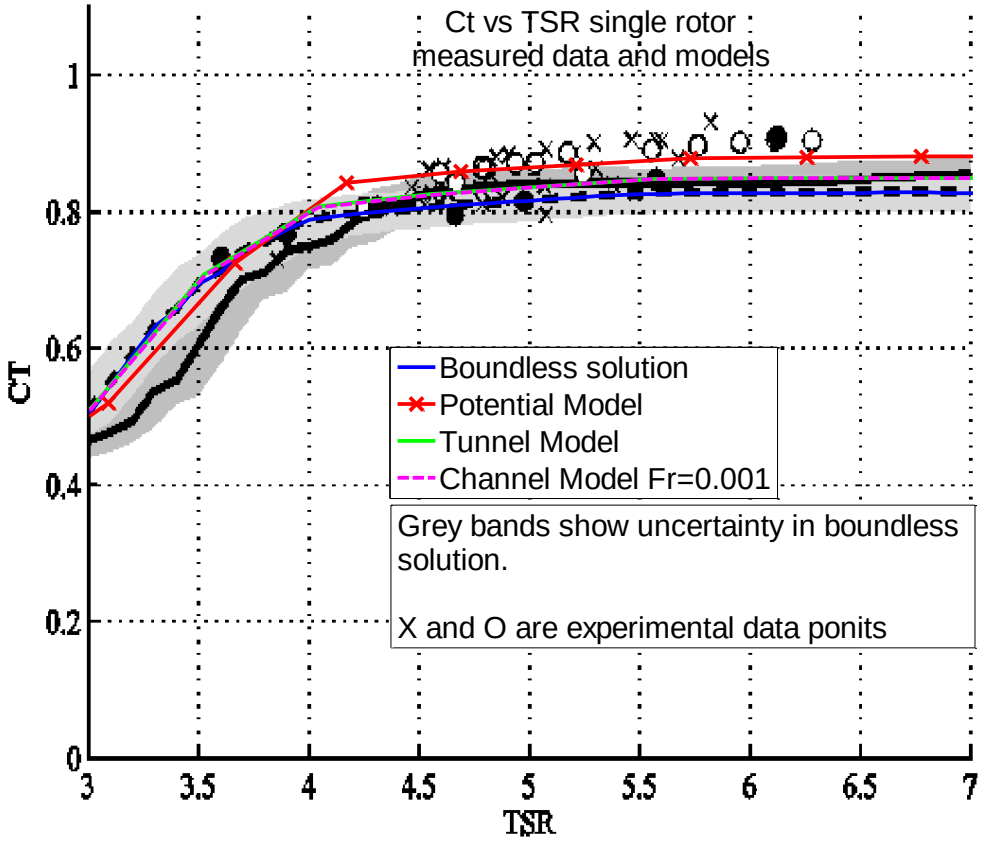

Figure 3-14: Comparison to 1/70th scale rotors (Ct vs TSR).

Some additional available data includes studies outside of PerAWaT. Whelan [2009] demonstrated the suitability of using 1-d corrected actuator disc theory for a highly blocked rotor comparing rotor thrust.

3.5 Single rotor performance in an array

Additional work undertaken within WG4WP2 measured the rotor thrust for different multiple rotor lateral spacings. The plot below shows how the potential model compares to the measurements Ct, Cp

vs lateral spacing. It can be seen that as the lateral spacing increases the increase in thrust reduces (as expected). The potential model correctly predicts a higher thrust on the central rotor compared to the outer two rotors.

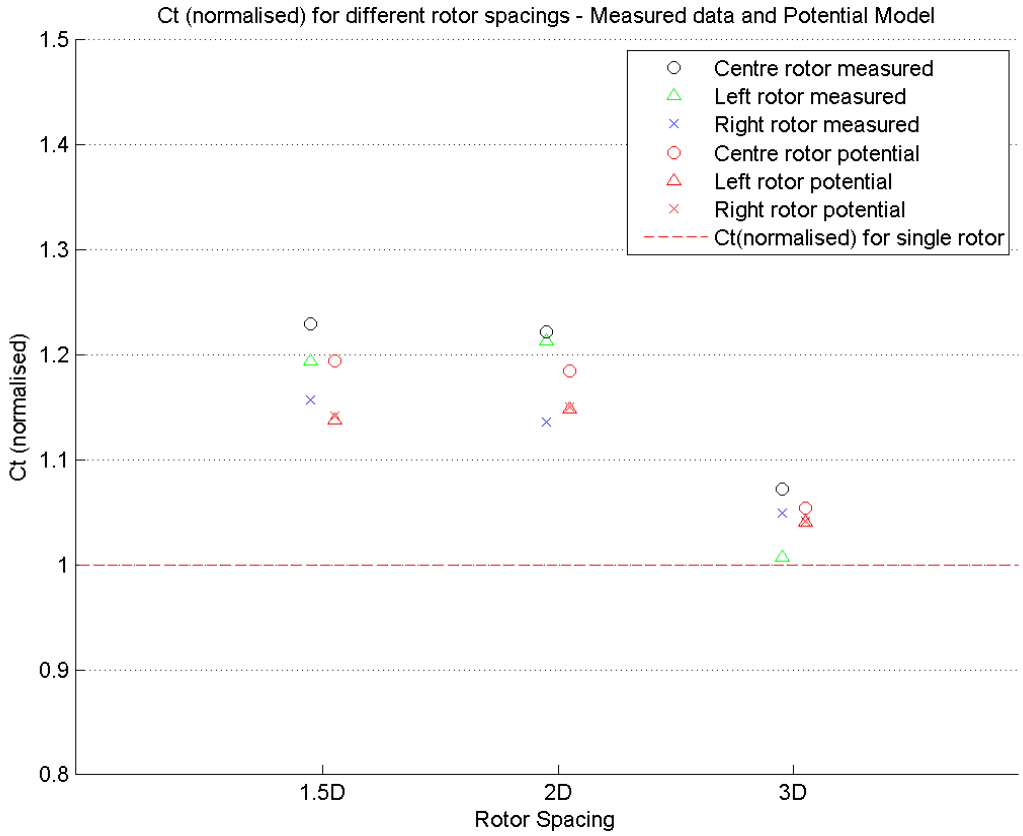

Figure 3-15: Three rotors at varying lateral spacing with measured and predicted values for the thrust coefficient.

3.6 Uncertainties associated with modelling assumptions

In order to assess the uncertainties associated with the modelling method a review of assumptions has been undertaken. The key modelling assumptions are:

- Steady flow – for the analysis of performance change, the flow speed is constant. This is on the basis that blockage impacts primarily upon the mean bulk flow and will not significantly change the dynamic characteristics of the rotor. Dynamic effects are incorporated by the use of measured Cp and Ct vs flow speed curves. The UoM data shows good agreement with the blockage model. This is assumed to be reasonable given the low frequency of tidal flow.
- Inviscid – the high Reynolds numbers mean viscous forces will be small, and that changes to performance will not be affected by viscous effects. If blockage acts to produce a large velocity gradient across the rotor, then viscous or turbulent stress forces might be

expected. However, the expected blockage ratios are sufficiently low that large velocity gradients are not expected.

- Irrotational – very little rotation is imparted into the wake flow, although the level of rotation is a function of the rotor design and the operating philosophy. The use of real rotor Cp, Ct curves means that the effect of such loss is propagated into the blockage model.
- The pressure driven expansion of the streamtube can be represented by a simple source term and characterised by the boundless Ct. More sophisticated models of rotors can be developed using potential theory. Such models provide more details of the distribution of flow field changes and would improve the absolute prediction of Cp and Ct. However, the blockage model is used to predict relative changes in performance and not the actual performance.
- The non-slip condition is not modelled, as it is assumed that the mean flow over the rotor is uniform, leading to a uniform change in flow outside of the streamtube. If an equivalent inflow is evaluated, then the mean effect is representative.
- The expected operational Froude numbers are low enough to ignore local surface disturbances. More detailed studies into this effect are required to evaluate the point at which the assumption becomes incorrect.
- Rotor resistance coefficient is independent of blockage. The measured data should make it possible to determine whether this is an appropriate assumption.

The potential flow model offers the ability to decouple lateral and vertical bounding effects. Verification of the model to 1-d analysis solutions shows that the error with the potential model increases from to about 5-7% at a blockage ratio of 20%, but is lower than this at lower blockage ratios. It is expected that a blockage ratio of 20% is at the higher end of practical deployment.

The model has been compared to the UoM experimental data and in the lower-blockage single rotor case the potential model performs well with only 2-3% error. In this case, where the vertical restriction drives the blocking effect the analytical solutions perform poorly. The potential model also performs well in the case of multiple rotors. In addition, the general trend of increasing and then levelling effect of reduced lateral spacings is well reproduced by the Potential model, with the order of error between 2-4%. To summarise, the blockage modelled is justified given the relatively small computational expense and the fact that good agreement with experimental data has been found.

The next step for model verification will be comparison to the CFD simulations which predict the change in Cp&Ct with blockage ratio and also different lateral and vertical restrictions. The experimental work planned under WG4WP3 will provide experimental data that can be used to further validate the model under a greater range of vertical restrictions.

4 NEAR WAKE MODEL

This section involves the description of the validation methodology for the GH near wake model and the comparison with experimental and numerical data that has been generated through the PerAWaT project. The models that have been developed were discussed in WG3 WP4 D2 (Thomson *et al*, 2010a) and the reader is referred to this report for the modelling details.

The near wake region has been discussed in some detail by (Vermeer *et al*, 2003). This is a region of complex flow characteristics. The centreline velocity retards causing the bounding streamtube to expand while vortices are shed from the blade tips. Given the relative complexity of the near wake, modelling the flow is not considered an option. Instead, the preferred strategy is to formulate some relationship between the known, environmental, geometric and operating conditions of the rotor with the velocity deficit generated through energy production. This information can then be fed into the far wake model (Ainslie, 1988).

As a consequence, the primary questions concerning the near wake are: how does one link the performance of the device with the velocity deficit and where does the near wake end? In answer to the latter, the near wake ends when the flow become self-preserving. A flow is said to be self-preserving (Tennekes & Lumley, 1972) if the flow is in a state of equilibrium where the inertia (convection of fluid) is dissipated through the shear stress (turbulent diffusion). In this situation the free-shear flow equations describe the motion and the wake profile is similar to a Gaussian curve.

At the point of self-preservation the turbulence can be related to the mean flow variables such as the initial velocity deficit and width of the wake. The effects of turbulent dissipation and production are considered to be unimportant such that vorticity is merely transported downstream. No attempt to model the energy cascade is made (Pope, 2010). Thus, modelling the various turbulent length scales is not vital in order to be able to afford an accurate description of the wake flow in the lee of a turbine.

To analyse the data in the near wake, a Gaussian profile will be fitted to the data. In combination with environmental conditions, the geometry of the experiment and the rotor performance the semi-empirical model can be validated for tidal flow. In addition, this allows (to some degree) the starting point of the far wake to be determined.

The findings of one study has suggested that these semi-empirical relationships still hold for tidal stream turbines and can therefore be applied (Myers *et al*, 2008). The purpose of the current study is to sample and summarise the near wake profile of the same device, operating at various thrust coefficients and ambient turbulence intensity values such that a semi-empirical formula may be derived which governs the flow dynamics of the near wake and determines the inflow conditions for the far wake model.

4.1 Brief description of model

It has been shown that, if the wake flow in the lee of an obstacle, is self-preserving, then the form of the velocity deficit can be taken to be Gaussian (Tennekes, 1972). Thus, it must be determined at what point the wake profile becomes self -preserving, in order for the Gaussian curve to give a good match with the data.

The near wake flow dynamics are complicated, however, the near wake is said to begin as soon as the shear layer is fully mixed through the centreline of the rotor. This can be identified by examining the lateral and vertical shear profiles. Once the end of the near wake is identified, the measured data are

fitted to a Gaussian profile. This allows the wake width, velocity deficit and centreline of the wake to be defined. From visual examination of the lateral velocity profile, we will be able to ascertain whether the same Gaussian shape applies to the near wake form in a hydrodynamic flow.

Once sufficient data has been collected on the operating and environmental conditions of the rotor then a semi-empirical formula can be determined. This formula will predict the velocity deficit and wake width of the wake flow. Given that these conditions will have to be determined for each of the different operating states, an understanding of the device under investigation is important. The performance of a ducted turbine, for example, may be different when compared to the three-rotor bare horizontal axis turbine. In summary, we expect that the near wake flow is dependent on the following physical quantities:

- Turbulence intensity.
- Type of rotor – flow differences for ducted and unducted.
- Blockage effects.
- Operating state, C_t, C_p.

The main assumptions of the near wake model are as follows:

- Turbulent – The kinematic viscosity of sea water is small and consequently the flow regime for a tidal flow during power production is a high Reynolds number. In fact, the Reynolds number is sufficiently large to assume that the flow will be turbulent.

- Incompressible - Incompressibility is a standard assumption in hydrodynamic flows and any density variations which do occur due to salinity or temperature variations may be neglected. These are small compared to other flow terms such as Reynolds shear and inertia.

- Inviscid – Away from solid walls the turbulent shear stress terms dominate over viscous effects. Therefore, it is assumed that the flow is inviscid.

- No boundary layer – The GH near wake model assumes that the inflow velocity profile has no shear in the vertical. This is linked to the assumption that the flow is unbounded. Shear will actually create an asymmetry in the vertical velocity profiles as the flow, in reality, is not uniform through the water column (as is shown in section 6). As a consequence, the measured data is normalised against inflow velocity. This allows us to directly compare a shear free wake profile with the GH Gaussian model.

- Self-preservation - The shear layer has met the centreline such that the fluid layer is well mixed and the flow deficit can be described using a Gaussian curve. In this situation the flow is self-preserving and the flow dynamics can be more attributed to the operating and environmental conditions of the rotor.

4.2 Validation methodology

In order to validate the GH near wake model we need to test how well the Gaussian profile matches with both experimental and numerical data. In addition, it is important to be able to predict the correct velocity deficit for a given operational condition i.e. Ct value. From Table 9 a list of all available experiments that can be used to validate the near wake model has been provided.

The main sources of information are the array scale experiments provided in WG4 WP1 and WG4 WP2. The array scale experiments provide transacts of the near wake profiles of each rotor. The

experiment was undertaken with only one ambient turbulence intensity value and the tip speed ratio of the devices was held constant. This is reflected in Figure 4-1 and Figure 4-2 where the operating point Ct varies between 0.6 and 0.9 while the ambient turbulence intensity values range over 6-8%. In addition, one experiment was run at a higher turbulence intensity. It is noted, that the lateral blockage of each test varied and therefore this covers some of the blockage parameter space (physical quantities, see section 4.1) desired for the near wake model.

In order to fully validate the near wake model, further experimental data is required at a range of thrust coefficients given realistic values for the ambient turbulence and blockage ratios. The second data set from WG4 WP1 will produce data for a bare horizontal axis turbine. These measurements will be performed at different tip speed ratios (and therefore Ct values) and the ambient turbulence intensity will be varied. In addition to the experimental data, we will also present preliminary results from numerical simulations performed in WG3 WP1.

Further experiments in WG4 WP3 will help parameterise the near wake model for a ducted turbine. The test schedule for these experiments is discussed in Stallard (2012). The primary interest will be in testing both the rotor and ducted turbine at different positions in the vertical to understand the impact on the near wake flow.

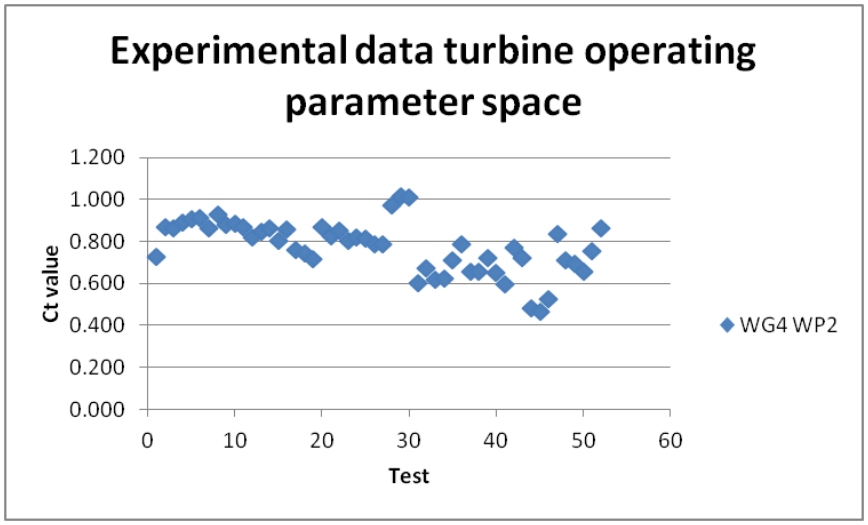

Figure 4-1: Operating points for the array scale experiments.

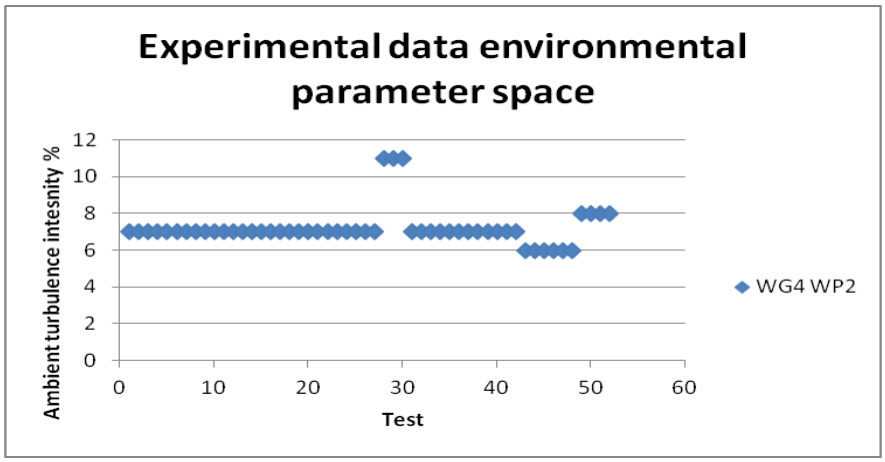

Figure 4-2: Ambient turbulence intensity values for the array scale tests.

4.3 Current validation

In the following sections we shall discuss the current work that has been undertaken to validate the near wake model. In particular, the experimental data available and the level of confidence we can attribute to predicting the velocity deficit will be discussed.

4.3.1 WG4 WP2 UoM Flume experiments

The graph of the Reynolds shear stress in Figure 4-43, gives an indication of where the near wake ends. Provided the curve of the Reynolds stress τ_{xy} passes through zero, with a linearly decreasing curve, then this shows that the shear layer has met the centreline such that the wake is fully mixed and can be described using a Gaussian curve.

In Figure 4-3 the shear stress curve tells us that the near wake has mixed fully and that the flow is self-preserving at this point. Therefore, we have taken measurements for the lateral and vertical velocity profiles and fit a 2-d Gaussian profile to the data, which has the following form

$$f = \hat{u}\, e^{\left(\frac{y-\mu y}{2\sigma y^2}\right)+\left(\frac{z-\mu z}{2\sigma z^2}\right)}. \qquad [1]$$

In drawing a comparison between the model and the experimental measurements an error analysis has been performed in order to estimate the error associated with modelling of the near wake. The error E is calculated using

$$E = \frac{1}{N}\left(\sum 1 - \frac{x_i}{y_i}\right), \qquad [2]$$

where y_i is the model predictions and x_i are the measurements.

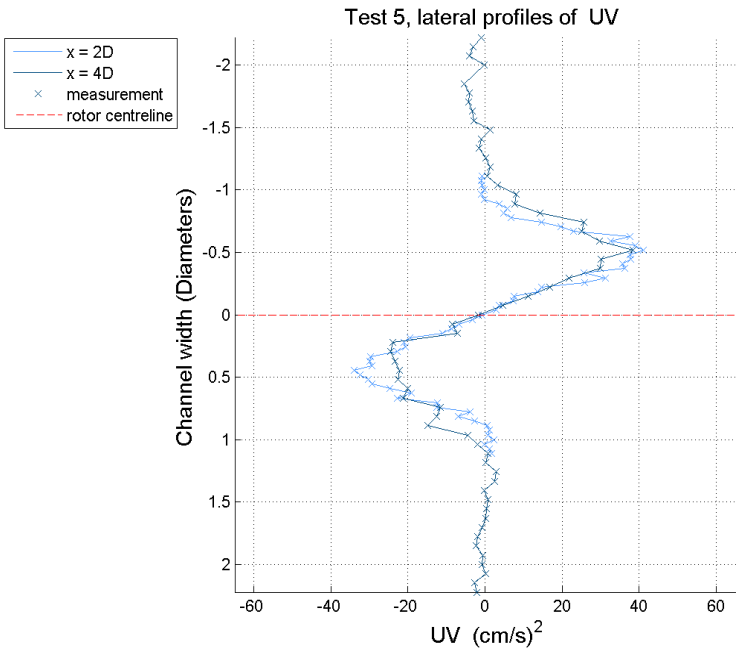

Figure 4-3: Reynolds shear stress profile $\boldsymbol{\tau_{xy}}$ downstream of the single rotor test case in WG4 WP2.

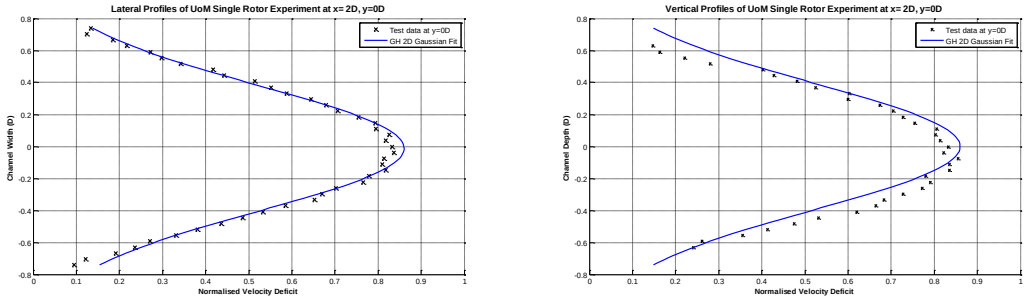

Figure 4-4: Lateral and vertical velocity deficit profiles for the single rotor test 05.

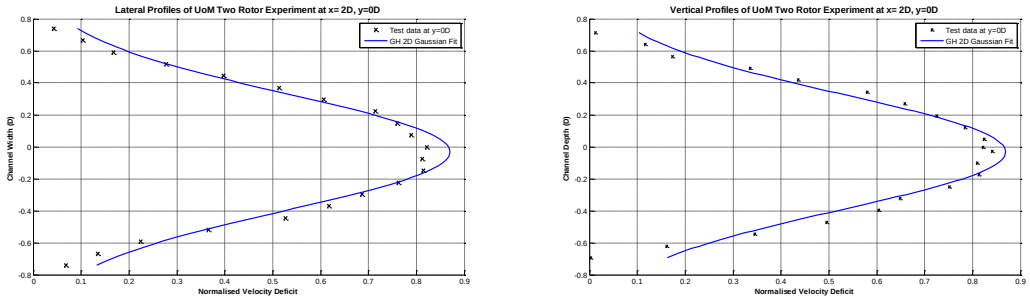

Figure 4-5: Lateral and vertical velocity deficit for rotor at y = 0 D in test 08.

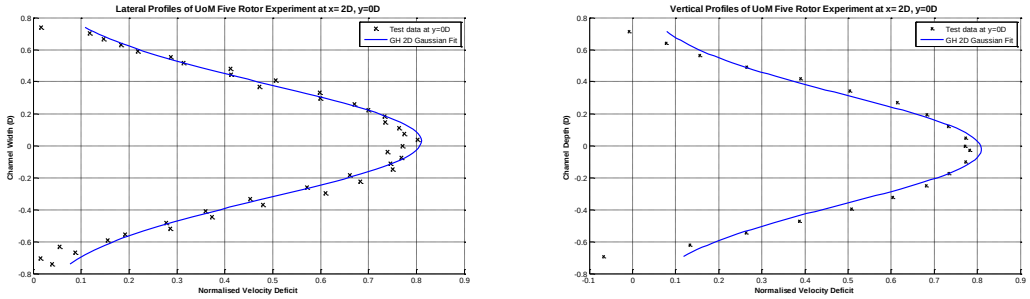

Figure 4-6: Lateral and vertical velocity deficit for rotor at y = 0 D in test 18.

Table 2: Summary of the Gaussian fit to the data for WG4 WP2.

Test case	Lateral Rotor position (D)	udefnor	μ y	μ z	σ y	σ z	Average Uncertainty E %			
							1D Lateral	2D Lateral	1D Vertical	2D Vertical
05	0	0.860	-0.011	0.000	0.393	0.395	5.14	5.09	10.18	10.18
06	0	0.853	-0.041	-0.040	0.374	0.357	9.05	8.91	13.47	13.69
06	1.5	0.839	0.060	0.033	0.371	0.351	10.00	9.99	10.76	10.78
07	0	0.863	-0.042	-0.033	0.364	0.354	10.03	10.04	15.38	15.86
07	2	0.837	0.036	0.019	0.357	0.346	9.23	9.35	12.20	12.23
08	0	0.873	-0.032	-0.031	0.365	0.361	10.50	10.49	14.29	14.38
08	3	0.813	0.051	0.006	0.356	0.347	8.79	8.35	10.22	10.04
09	0	0.825	-0.008	-0.012	0.350	0.337	10.25	10.28	10.43	10.52
09	1.5	0.783	0.094	0.002	0.340	0.324	13.36	13.26	15.55	16.20
09	-1.5	0.821	-0.087	-0.038	0.345	0.340	8.57	8.90	13.64	13.63
10	0	0.858	-0.018	-0.023	0.346	0.335	11.37	11.16	12.35	12.36
10	2	0.841	0.051	0.011	0.350	0.340	13.83	13.75	10.19	10.46
10	-2	0.843	-0.091	-0.025	0.354	0.338	11.54	11.61	11.32	11.45
13	0	0.873	-0.010	-0.034	0.384	0.387	12.16	12.08	11.43	11.29
13	1.5	0.824	0.086	0.028	0.350	0.336	14.54	14.57	12.33	12.05
13	-1.5	0.837	-0.085	-0.036	0.358	0.334	12.86	13.11	13.44	13.60
15	0	0.781	0.003	-0.009	0.462	0.432	4.51	5.10	5.62	5.57
15	1.5	0.738	0.084	0.008	0.465	0.416	6.08	5.98	5.52	6.44
15	-1.5	0.769	-0.063	0.004	0.447	0.403	3.48	3.75	4.60	4.72
18	0	0.812	0.029	-0.022	0.354	0.342	10.72	10.82	10.75	10.74
18	1.5	0.801	0.090	0.033	0.353	0.347	14.98	14.97	11.05	11.29
18	3	0.803	0.166	0.013	0.353	0.343	25.00	25.12	11.12	11.14
18	-1.5	0.813	-0.048	0.005	0.356	0.323	10.83	10.71	12.48	12.36
18	-3	0.856	-0.066	-0.026	0.372	0.348	6.81	6.92	13.37	13.54
19	0	0.761	0.011	-0.005	0.409	0.389	6.10	6.12	7.30	7.26
19	1.5	0.856	-0.066	-0.026	0.372	0.348	8.86	8.45	11.73	11.74
19	3	0.760	0.105	0.014	0.434	0.414	11.85	12.59	8.86	8.79
19	-1.5	0.711	-0.070	0.002	0.451	0.375	3.06	4.46	14.55	11.96
19	-3	0.775	-0.047	0.007	0.421	0.385	2.14	3.00	5.15	5.54
20A	2.25	0.807	0.059	0.014	0.405	0.391	3.38	5.42	8.28	8.19
20A	0.75	0.733	0.020	0.003	0.447	0.381	3.08	3.07	7.12	7.24
20A	-0.75	0.635	-0.033	-0.013	0.449	0.380	3.10	2.90	8.09	8.40
20A	-2.25	0.795	0.029	0.005	0.396	0.382	3.32	4.05	6.88	7.10
21	0	0.613	0.005	0.014	0.634	0.465	13.38	13.06	11.81	11.92
21	1.5	0.550	0.005	0.003	0.659	0.468	3.98	4.25	3.38	3.37
21	3	0.775	-0.025	0.017	0.475	0.414	3.98	4.34	5.28	5.37
21	-1.5	0.542	-0.007	0.017	0.660	0.484	3.84	3.83	4.15	4.15
21	-3	0.795	0.061	-0.017	0.402	0.383	9.24	9.65	9.19	9.11

Results of fitting 2-d Gaussian profiles to the data have been provided in Figure 4-4, Figure 4-5, Figure 4-6. It is clear to see that the Gaussian profile is in excellent agreement with the experimental measurements of the normalised velocity deficit in the lateral direction.

In the vertical, there is an asymmetry that is caused by the shear layer. In order to compare against experimental measurements the velocity deficit is found by normalising against the vertical inflow profile. This effectively `removes' shear from the data and allows us to find a fit with the Gaussian

profile. Although the seabed violates the assumption that the flow is not close to a solid wall boundary and therefore is not inviscid, good agreement is still found using the Gaussian profile in this case.

Table 2 gives a summary of the parameters found when fitting a 2-d Gaussian surface to the flow measurements. This data can be used to assess the capability of the GH near wake model or to find a parameterisation that will predict the wake width and velocity deficit given information concerning the operating, environmental and geometric conditions of the flow field and rotor. In addition, an error analysis is provided that estimates the deviation of the measured data from model predictions using equation 2. The error is generally low therefore it appears that the Gaussian profile, given by equation 1, is adequate when describing the shape of the near wake profile.

4.3.2 WG4 WP1 EDF flume experiments

The EDF single device scale experiment examined the wake structure of a single rotor device (Buvat *et al*, 2012). The flow readings were taken for a variety of different flow states (turbulence condition, flow velocity) and at different operating conditions (varying TSR). These are summarised in Table 9.

Results from the first test, that of channel depth of h = 0.8m, free-stream flow speed U_o = 0.27 and turbulence intensity I_{amb} = 5 % are provided in Figure 4-7 and Figure 4-8 we see that the high blockage ratio (see Table 9) in the lateral direction causes large flow acceleration around the turbine. In particular, the situation is compounded by the proximity of the sidewalls. This makes the flow dynamics very complicated as was discovered in Buvat (2010b).

Just like the seabed creates a boundary layer, so do bounding sidewalls such as in the single rotor experiment. The turbulence structure in a boundary layer is complicated due to interactions with the viscous sub layer and the turbulent flow. In fact, it is the generation of shear which drives turbulence. In this case the sidewalls will energise turbulence in a way that would not occur if the device was operating in an unbounded flow. The GH models that have been developed to describe wake flow assume that there are no bounding side walls and that drag is created only from devices in an unbounded domain. In general the near wake description does not work as well in the vertical because of the presence of a boundary layer. This was noted in section 4.3.1 where there is an asymmetry in the vertical profiles. In this case, it is likely that we will see limitations in the performance of the near wake model when considering the lateral profiles. This is possibly the upper limit when considering blockage ratios in a flume and we need to bear this in mind when analysing the data.

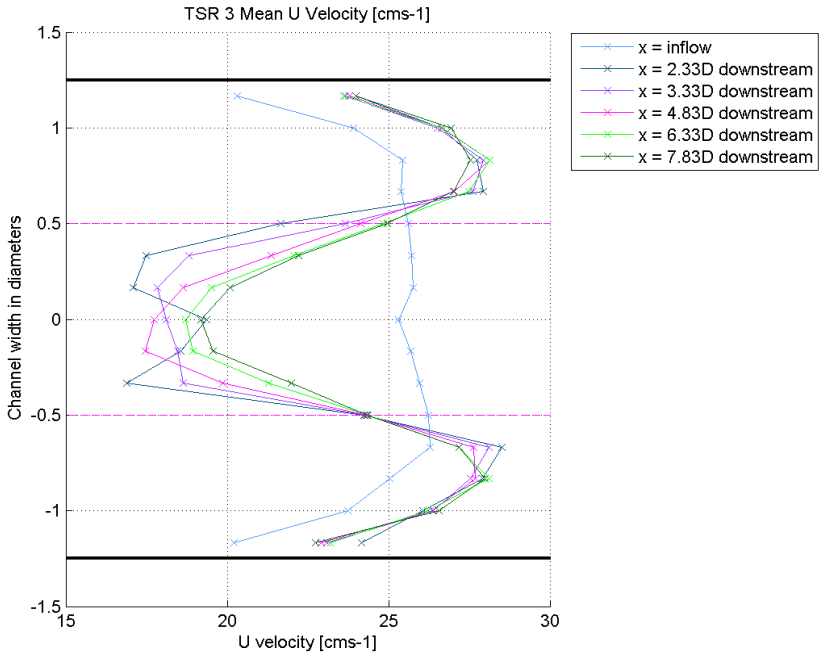

Figure 4-7: Streamwise velocity profiles of the fluid flow in WG4 WP1 at various downstream positions for TSR = 3, in test 1

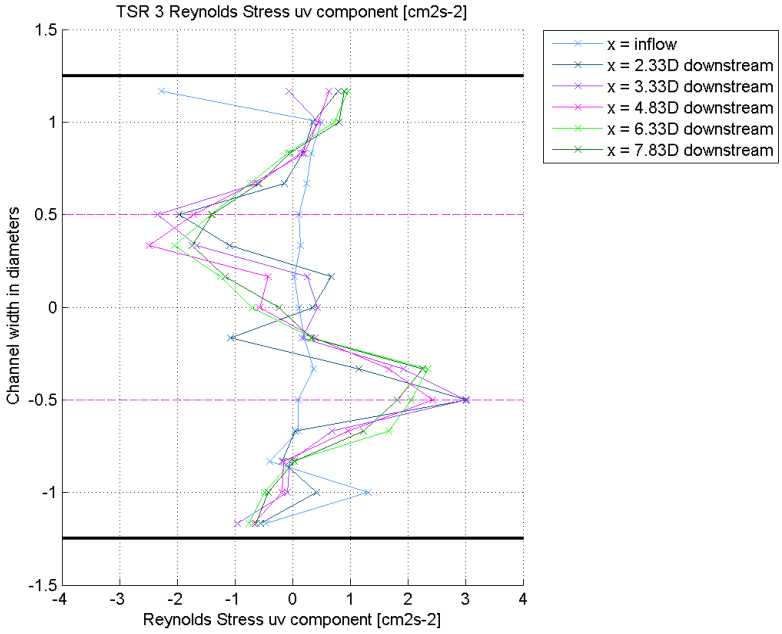

Figure 4-8: The Reynolds shear stress τ_{xy} at various downstream positions for test 1 of WG4 WP1.

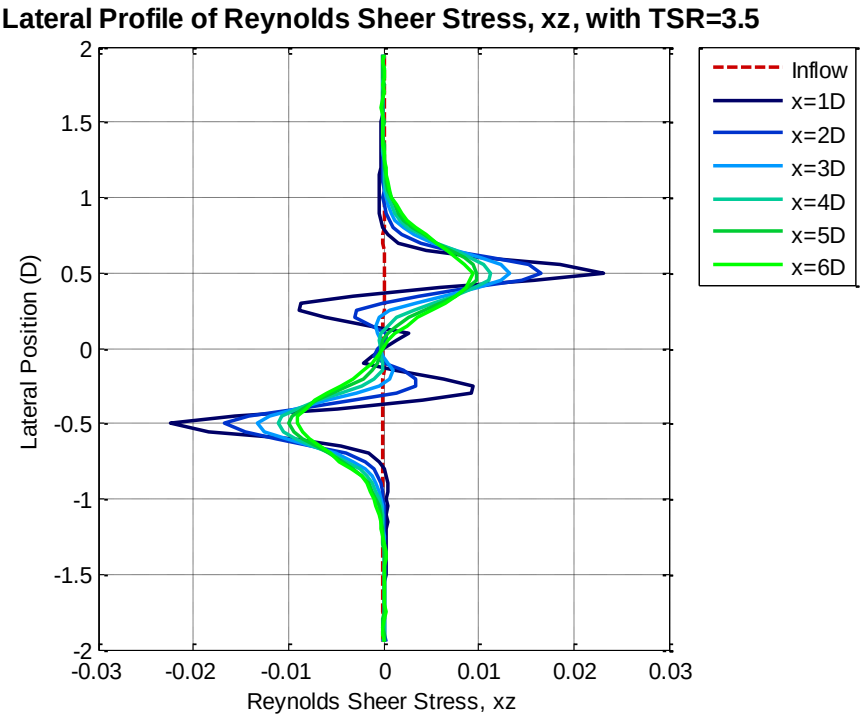

Figure 4-9: Reynolds stress profile from numerical experiment results in WG3 WP1.

From the profiles of the Reynolds stress in Figure 4-8 it can be seen that the shear layer does not reach the centreline until sometime after 5D downstream. This is in stark contrast to the experiments in WG4 WP2 where the shear layer suggested the near wake ended around 2D downstream.

4.3.3 WG3 WP1 UoO Single rotor numerical work

The `base case' from the numerical simulations undertaken by the UoO is presented in Figure 4-9. Here the numerical model has been validated against the EDF single rotor. These results have been obtained using a blade element momentum model of a single device embedded in a CFD package. For a similar tip speed ratio (3.5) as the EDF experimental results shown in Figure 4-7, Figure 4-8, only after 6D does the shear layer reach the centreline. The shear profile is a measure of how much the velocity is changing. If the value is zero, across the rotor disc then these is no change in the flow velocity. In both cases we see that the shear profiles at around 1D have sharp peaks. This represents a sudden change in the flow velocity. As the flow develops the curve smooths out until there is a continuous profile. Eventually we see that the shear stress is linear through the centreline, showing a gradual change in the flow velocity at this point.

For both the blade resolved and embedded BEM CFD model simulations have been performed with the rotor speed and pitch angle held constant. However, simulations for a range of (time averaged) rotor characteristics i.e. Cp, Ct vs TSR are performed. In practice 'real' rotors would have a closed loop control system that would result in variations in rotor speed (and pitch angle) with time.

4.4 Conclusions, critique and further work

Near wake profiles from experimental measurements taken in WG4 WP2 have been compared to Gaussian profiles. Excellent agreement has been found in the lateral and vertical directions. A table of

results summarising the velocity deficit, and wake width has been produced. This will allow a comparison between existing models that predict the velocity deficit or the opportunity to develop new models.

The experimental data available through WG4 WP1 was discussed. It was concluded that the blockage ratio was high for a tidal stream turbine and that any analysis performed on this data set should be considered carefully.

The results form numerical simulations in WG3 WP1 will be processed and a comparison formed with the near wake model results. In addition, the results from experimental work in WG4 WP3 will be analysed as and when they are made available.

A discussion of the validity of the model assumptions is provided below:

- Turbulent, Incompressible, Inviscid – The Gaussian profile used in the GH near wake model to determine the wake width is derived under the assumption that the flow is turbulent, incompressible and inviscid (Tennekes & Lumley, 1972). This model fits well with preliminary results and therefore the approach appears well justified.

- No boundary layer – The agreement with the Gaussian profile has been found to be good in both the vertical and lateral profiles. However, further understanding of how the boundary layer affects the near wake flow is required before we can be confident in the results. The experiments that will be carried out in WG4 WP3 will aim to understand the effect on the near wake flow, for a device, when vertical position is varied. This will help further understand the limitations and applicability of the current GH near wake model. In addition, the numerical simulations in WG3 WP1 will also be useful for cross verification purposes.

- Self-preservation – As was shown for the array scale experimental results the shear layer has met the centreline such that the fluid layer is well mixed. Hence, the flow deficit can be described using a Gaussian curve. In this situation the flow is self-preserving and the flow dynamics can be attributed to the operating and environmental conditions of the rotor.

5 FAR WAKE MODEL

In order to predict inter array effects of a series of tidal stream turbines, the velocity deficit imposed on the flow due to upstream turbines must be predicted accurately. Here, we discuss the far wake model which calculates the rate of recovery of the flow velocity after energy has been extracted.

The far wake model is based on the drag that is generated when flow moves passed a bluff body in an unbounded domain. In this case, the wake blockage generated by an operational turbine replicates the drag generated from a blunt body. This phenomenon can be modelled using the free-shear layer equations (Anderson 1995, Tennekes & Lumley, 1972).

These equations assume that the flow is self-preserving such that the turbulence is in local equilibrium. In other words, the turbulence can be related to the mean flow variables such as the initial velocity deficit and width of the wake. The effects of turbulent dissipation and production are considered to be unimportant such that vorticity is merely transported downstream. Thus modelling the turbulent length scales is not vital in order to be able to afford an accurate description of the wake flow in the lee of a turbine.

In addition, the far wake model is not specific to any particular device, and so can be applied to model a ducted and open centre device as well as the bare horizontal axis turbine.

5.1 Brief description of model

TidalFarmer utilises two different wake models that have been developed by GH and applied to model array interactions. The first is a standard model that has been successfully applied in the wind industry. It is an axisymmetric description of the wake deficit and uses the eddy-viscosity turbulence closure model described in (Ainslie 1988). The second model has been developed as part of the PerAWaT project and, while computationally efficient, offers an advantage in terms of the wake mixing of multiple turbines. For more detail the reader is directed to the earlier PerAWaT deliverable (Thomson *et al*, 2009). By simultaneously developing new models and retaining pre-existing models and adapting them to meet the demands of tidal stream turbine technology the user can be confident in the energy predictions calculated by TidalFarmer.

The 2-d and 3-d eddy-viscosity models are based on the free-shear layer equations (Tennekes & Lumley,1972). For energy extraction, we are interested in the wake flow of a bluff body, such as that of a turbine. This system of equations is derived on the following assumptions:

- Turbulent – The kinematic viscosity of sea water is small and consequently the flow regime for a tidal flow during power production is a high Reynolds number. The Reynolds number is sufficiently large to assume that the flow will be turbulent.

- Incompressible – This is a standard assumption in hydrodynamic flows and any density variations which do occur due to salinity or temperature variations may be neglected. These are small compared to other flow terms such as Reynolds shear and inertia.

- Unbounded – The flow is assumed to be in an unbounded domain such that the equations model the decay of turbulence.

- Inviscid – Away from solid walls the turbulent shear stress terms dominate over viscous effects. Therefore, it is assumed that the flow is inviscid.

- No boundary layer – The model is run assuming that the inflow velocity profile has no shear in the vertical. Again this is linked to the assumption that the flow is unbounded. Shear will actually create an asymmetry in the vertical velocity profiles as the flow, in reality, is not uniform through the water column (as is shown in section 6). It is argued that modelling the boundary does not produce significant error as the device will typically be located in the higher region of the boundary layer where there is less shear.

- Self - preservation – Once the flow is sufficiently far downstream, the flow is in a state of equilibrium where the inertia (convection of fluid) is dissipated through the shear stress (turbulent diffusion). If this condition is satisfied then the flow is said to be self-preserving and the free-shear layer equations model the flow well. Hence, the point at which to start the far wake is important, as the model does not recreate the physics close to the turbine.

- Eddy-viscosity model – The primary assumption of the far wake models lies in the turbulence model that has been adopted. The eddy-viscosity assumes that turbulent dissipation mimics molecular diffusion. This is a valid assumption, provided that turbulent eddies are not stretched or compressed and are merely transported downstream. In the case of free-shear flow such as the wake of a turbine this is a valid assumption as the flow is self-preserving. In this situation, the turbulent properties are dependent on the flow variables and therefore the flow is in local equilibrium.

The far wake models have effectively two tunable parameters. The eddy-viscosity turbulence closure model is one tunable parameter (Tennekes, 1972) and the second is where the far wake model starts. This has been found to be anywhere between 1-5D (Crespo & Hernandez, 1996). Once the wake start is chosen the eddy-viscosity parameter can be fixed. The eddy-viscosity is in fact dependent on the length and velocity scales of the flow (including the turbulence intensity) but suitable parameters must be chosen to fix the effective wake mixing.

Table 3 gives a number of input parameters that form part of the far wake models and the effect that these inputs will have on the form of and shape of the far wake. These parameters were described in Thomson, et al (2010).

The 3-d model is solved on a Cartesian mesh which is aligned to the streamwise flow direction such that lateral flow gradients are small. This is believed to be acceptable given that for energy extraction, a uniform flow will be desired (Garrett & Cummins, 2005). The 2-d model solves the equations for an unbounded axisymmetric streamtube. Therefore, it is anticipated that these two models will provide different results given that boundary conditions will influence the computation. The mixing length model or eddy-viscosity model is parameterised differently in both models. This is detailed in (Thomson, *et* al, 2011c). However, both models have the same inputs parameters to model the turbulence.

As the 3-d model solves the entire flow field, the merging of multiple wakes is obtained as part of the solution. However, the 2-d model only calculates the velocity deficit for a single rotor. Therefore, a further algorithm is required in order to combine wakes from separate turbines. The following algorithms have been adopted for the GH far wake models (Thomson *et al*, 2011b), a linear superposition, largest deficit, and the root mean square. These effectively blend the downstream wakes together with no attempt to model interactions.

Table 3: List of input parameters for the the 2-d and 3-d eddy-viscosity model and there impact on the model results.

Input parameter	Description	Sensitivity
F_{k1}	Controls mixing through the shear layer due to large scale eddies.	Has a large impact on the rate of decay of the wake.
I_{amb}	The turbulence intensity controls the mixing which occurs due to ambient turbulence generated from external factors such as seabed roughness, headlands etc.	Has a large impact on the rate of decay and shape of the wake.
s_0	This is the point at which the far wake model is said to model the flow.	It is important that this parameter is chosen correctly otherwise the model will be applied to flow measurements it cannot reproduce.
C_t	The corrected thrust value as described section	This will alter the magnitude of the velocity deficit.

5.2 Validation Methodology

In order to validate the far wake model it is intended that the following comparison with experimental data must be performed, as described in (Duckworth & Barthelmie 2008):

- The centreline velocity deficit of a single rotor wake.
- The wake width and shape in comparison to experimental data.
- The shape of lateral and vertical flow profiles.
- Different ambient turbulence intensities must be considered.
- The wake added turbulence.
- The models should be compared to experimental data where the devices are operating at different thrust coefficients.
- The impact of wake meandering on the flow.
- Consideration of different blockage ratios.
- Investigation of combination of multiple rotors and the wake merging that will occur as a result.

In the following sections the model will be compared against several experiments undertaken by the University of Manchester for which a summary has been given in Table 9. A further comparison will be made using the results provided in both WG4 WP1 and WG4 WP3. However, it is not clear how useful the results from WG4 WP1 will be, given that the close proximity of bounding walls will contravene the assumption that the flow is unbounded.

5.3 Multiple rotor flume data (WG4 WP2)

In order to validate the wake model described in Thomson *et al,* (2011) a flume experimental study at the University of Manchester has been undertaken. The primary objective of this study was to understand the effect of boundary conditions on the wake structure of several turbines while operating in close proximity in different arrangements.

Turbine configurations which were of interest included a turbine whose wake was constrained on one or both sides by the wake of an adjacent device. Further studies of interest were increasing the array size laterally to encompass up to five operational devices and then additional rows. Furthermore, the investigation of staggered array layouts where a downstream device is partially within the wake of an upstream device and the variation of lateral and longitudinal spacing were considered to be important factors which also require investigation.

The study also included the effect of ambient turbulence upon wake mixing. Seabed roughness at the inflow of the flume produced a turbulence intensity of around 10%. However, as the flow developed downstream it was found that the turbulence intensity dropped to around 8%. One of the input parameters for the eddy-viscosity model is the ambient turbulence intensity. Therefore, in the present study the input for intensity will be varied over this range when making a comparison with the measurements.

5.3.1 Centreline velocity deficit

To calibrate the eddy-viscosity model, the drag term F_{k1} which is described in (Thomson, 2011c), will be specified. This is done for both the 2-d and 3-d wake models to compare with the single rotor test case 05 of WG4 WP2. This allows us to fix the parameter which determines wake mixing due to the shear layer turbulence. The other parameter to be determined is the wake start. As mentioned previously, this point needs to be aligned with the end of the near wake. The exact start point is still unknown and depends on multiple factors (Vermeer, *et al* 2003). For this simulation it was decided that the best choice would be to start 2.5 D downstream. A sensitivity study where the wake start position was varied and the error estimated using equation 2, shows that this is in fact the best place to start the far wake model, see Figure 5-16. Table **4** summarises the error associated with each wake start position. Finally, the value of the turbulence intensity was chosen to be 10%.

Figure 5-1 shows a comparison between the UoM single rotor experiment (Test 05) and the GH 2-d and 3-d far wake models. Matching with the centreline velocity deficit is imperative in order to understand whether the model is correctly predicting the wake decay. It is clear to see that the velocity deficit is matched well by the eddy-viscosity models which solve the simplified free-shear layer equations. In particular, the 3-d model provides a good fit over the course of the wake.

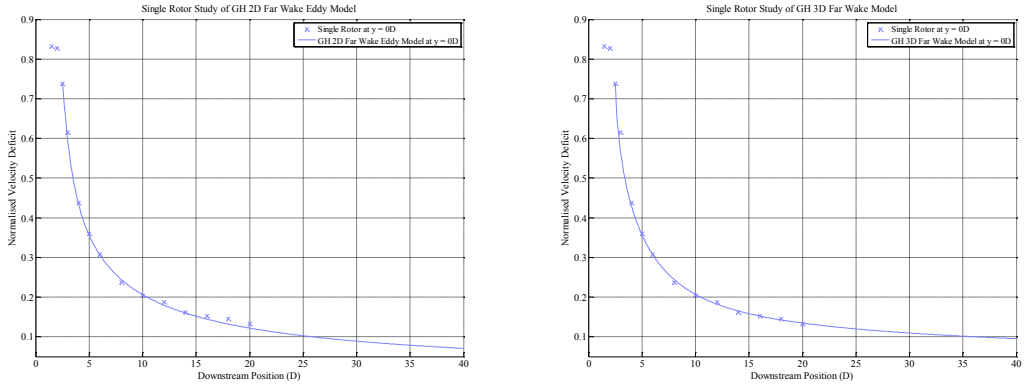

Figure 5-1: Measurements of centreline velocity deficit directly behind single rotor compared to 2-d and the 3-d eddy models in test 05.

From an economic perspective, ideally, turbines would be placed closely together. Therefore, it is important that the velocity deficit between 5D-15D is well modelled. In Figure 5-1 we can see that in this region, both models match the data well.

The next question is how well the shape and width of the flow profiles compare to the experimental data. In Figure 5-2 and Figure 5-3 the 2-d and 3-d models are compared to the flow profiles in the lateral and vertical directions. Here we find that there is very good agreement between the experimental and GH model prediction at 4D downstream of the device. The wake shape of the 3-d model appears to be marginally better than the 2-d form. In addition, the asymmetry due to the neglect of the vertical boundary layer can be seen in the comparison in the depth profile.

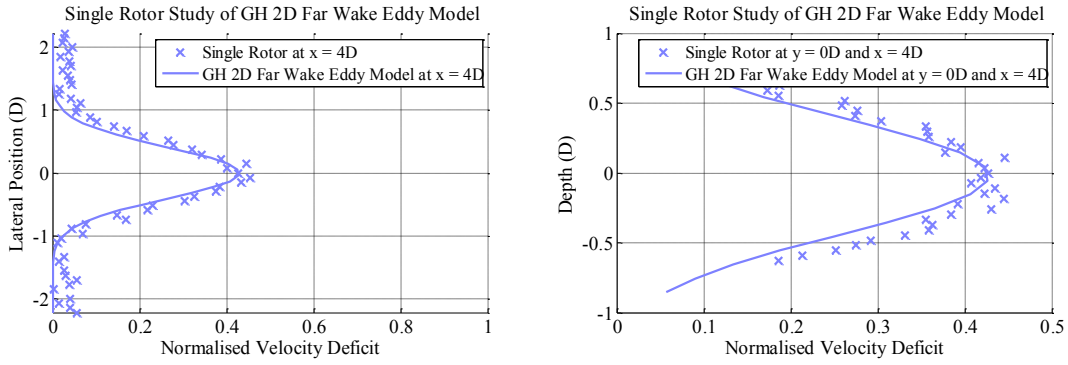

Figure 5-2: Comparison with the 2-d model to experimental measurements of the wake width and shape in test 05.

At present more data is required for turbines operating at different thrust coefficients. This should be assessed in the single device experiments performed in the EDF flume in WG4 WP1 and WG4 WP3. This will allow confidence that wake decay growth is predicted for a variety of operating states throughout the tidal cycle. Further cross verification can be performed against the numerical studies undertaken in WG3 WP1, WG3 WP5 and ReDAPT.

5.3.2 Shape and width of the lateral and vertical flow profiles

In this section we wish to discuss the predictions of the wake model when examining the vertical and lateral profiles of the flow. This is strongly linked to the ambient turbulence intensity. In a turbulently energetic flow we expect that the wake width will increase faster as the rate of mixing is larger and the wake disperses quickly. Here we examine each of the models in comparison to, once again, the UoM single rotor test case. It is noted that both the profiles in the lateral and vertical have been normalised to the inflow profile such that a direct comparison is made with the axisymmetric wake models which assume the inflow profile is uniform.

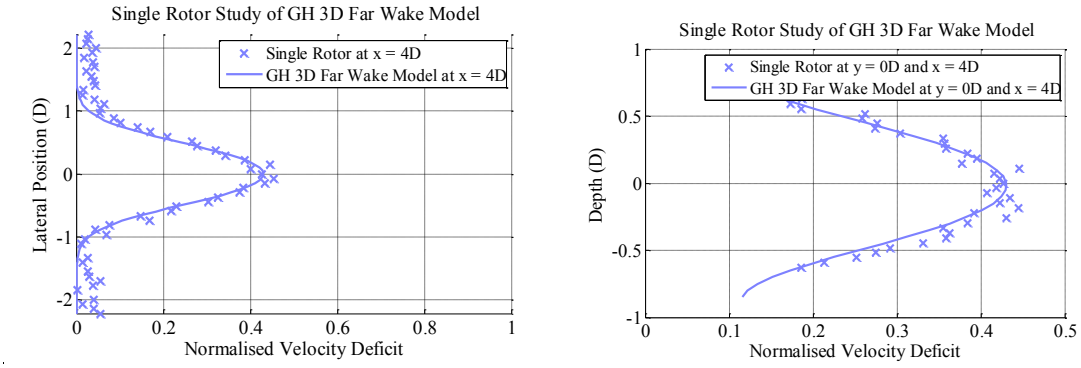

Figure 5-3: Comparison with the 3-d model to experimental measurements of the wake width and shape in test 05.

In Figure 5-2 the lateral velocity deficit is well predicted by the 2-d eddy model at a distance of 4D downstream. This suggests that both velocity deficit and wake width have been well predicted. One interesting point to highlight is the manner in which the flow deficit is calculated using the 2-d model. This was described in the report by Thomson, et al (2011b). It was noted that the bounding effect of the free-surface could `squash' the wake profile so that rather than being cylindrical, as assumed in the axisymmetric model (2-d eddy), the cross section is in fact elliptical. While this does not cause any issues with respect to conservation of mass it has caused problems with respect to the wake width agreement in the lateral and vertical profiles. Instead, it appears that depth limited nature of the flow does not appear to have such a pronounced effect on the shape of the wake width and therefore any adjustment to the wake shape is not required.

Figure 5-3 presents the shape of the vertical and lateral profiles calculated from using the 3-d eddy model. Once again the results match well with the flow measurements. Further features to note are the slight asymmetry in the vertical profile shown in Figure 5-2 Figure 5-3. However, this deviation is clearly small. Therefore, it is not a priority to add a boundary layer profile for the depth.

Further work would include flume experiments where the turbulence intensities are varied such that the effect upon the wake width and shape can be analysed in more detail.

5.3.3 Combination of multiple rotors operating in a flume

In this section we wish to address the effects of wake mixing and merging of multiple devices. The importance of being able to merge multiple wakes and how they interact is important when

considering the loss in energy to flow speed reduction and the hydrodynamic loading of structures due to turbulence (Ainslie, 1988). The experiments in Thomson, *et al* (2011a) have focused on the wake mixing of several turbines operating in multiple rows.

In Figure 5-4 we have a comparison between the centreline velocity deficit of two rotors operating side by side. In this test case we have in fact used a value for the turbulence intensity of 9%. This is seen as a sensible value as the ambient turbulence intensity decreased as the flow moved downstream. A lower value for the ambient turbulence intensity will reduce the rate of decay of the velocity deficit and consequently leads to a slower recovery. It is also interesting to observe how sensitive the model is to changes in input variable. In this case the 2-d and 3-d models both slightly over-predict the flow deficit. As the flow moves passed 4D downstream.

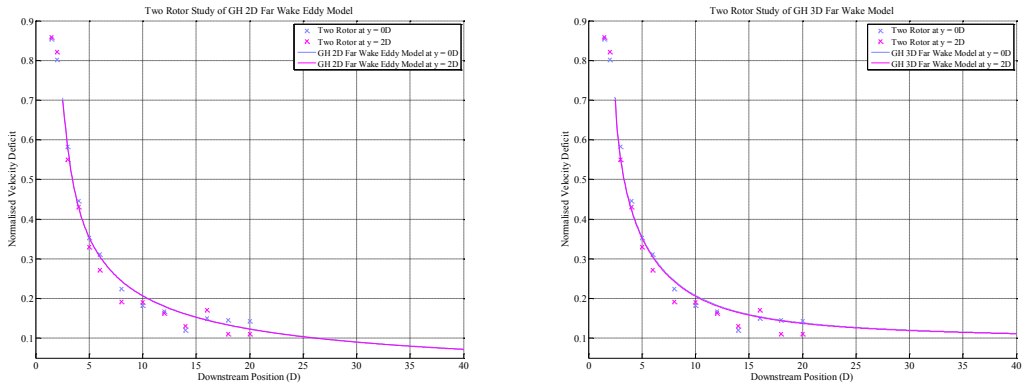

Figure 5-4: Comparison of the velocity deficit of two turbines operating in a row from test 07 with the 2-d and 3-d models.

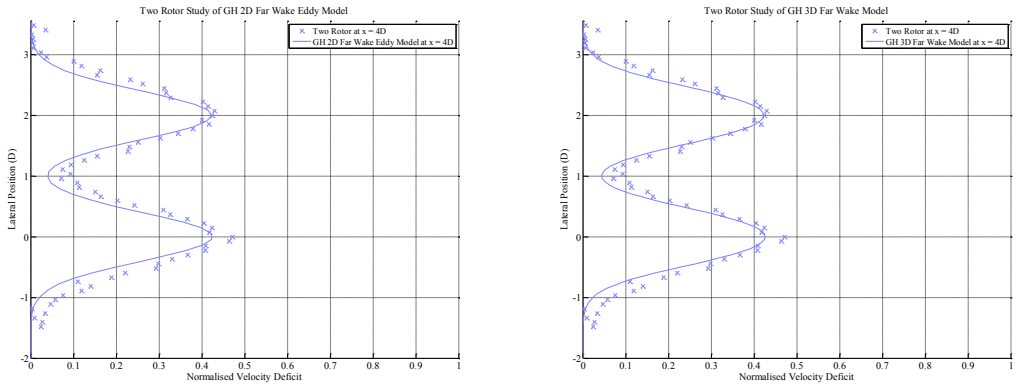

Figure 5-5: Comparison of the lateral velocity deficit from test 07 and the GH far wake models. For the 2-d model the wakes were merged using the linear superposition algorithm.

With respect to the wake width and the lateral velocity profiles, it is found in Figure 5-5 that agreement is very good. In particular, that wake mixing of both models is shown to produce good results. Here the wake merging algorithm that was chosen uses linear superposition (Thomson *et al*, 2011b) in order to blend the different wakes together. Two further algorithms are considered in Figure 5-6 and Figure 5-7 the largest wake deficit and root mean square algorithms have been implemented in order to obtain the lateral velocity profile. Here we see that both give slightly smaller velocity deficits than linear superposition. In addition, the root mean square gives a sharper wake profile near the meeting point of both wakes.

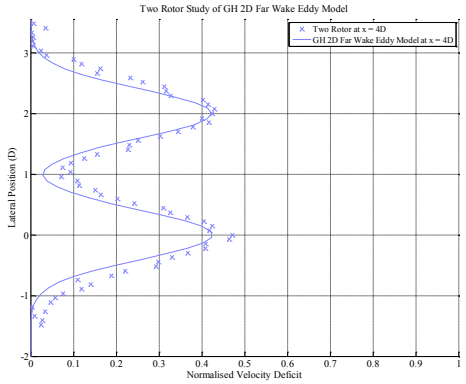

Figure 5-6: Comparison of experimental data from test 07 with wakes merged using a root mean square algorithm.

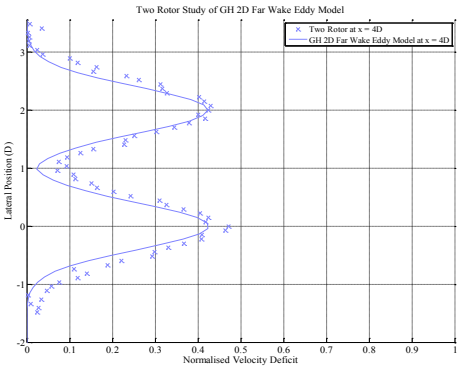

Figure 5-7: Comparison of experiment data from test 07 with wakes merged using the largest deficit algorithm.

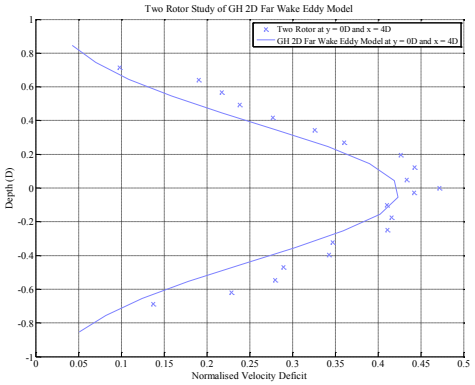

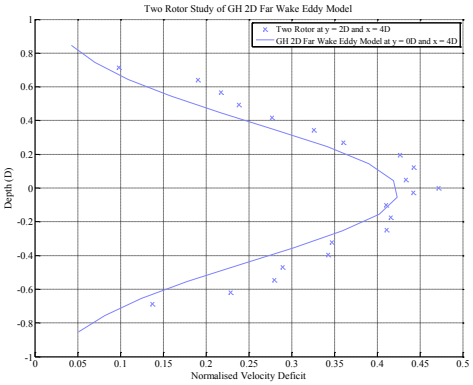

Figure 5-8: Comparison of the velocity deficit from test 07 in the vertical at $\boldsymbol{y = 0}$D for the GH 2-d wake model.

Given that it is only the velocity deficit at the edges of the wake that are merged the solution towards the centreline will remain unaffected. In Figure 5-8 and Figure 5-9 we present the vertical velocity

profiles of the two rotor centrelines for the 2-d and 3-d eddy wake models. Once again, the predictions match well with the experimental data in both cases.

The model has performed well for two rotors with a separation of 2D. The primary focus of the models has been to examine wake mixing close to the turbine at 4D. In test 13 performed by (Thomson *et al*, 2011a) an investigation of three rotors operating at 1.5D lateral separation was undertaken. Readings of the lateral profiles were taken at multiple points downstream that give a source for comparison against the 2-d and 3-d models.

The ambient turbulence intensity adopted for this set of simulations was 8%. From Figure 5-10 and Figure 5-11 the centreline velocity deficit is presented for the 2-d and 3-d eddy models. The 3-d model distinguishes well between the velocity deficit of the central rotor, operating at y = 0D, and the adjacent rotors. In contrast, the 2-d model does not capture the difference in deficit quite as well.

In Figure 5-12, Figure 5-13, Figure 5-14 and Figure 5-15 the lateral profiles are compared to the experimental data at several points downstream. It is clear to see that the 3-d wake model consistently predicts a higher velocity deficit in gaps between rotors. This is in good agreement with measurements taken in the flume.

Comparison between measured data taken downstream of the central rotor and the vertical deficit calculated using the GH 2-d and GH 3-d wake models have been included in Figure 5-17, and Figure 5-18. Here we can see that the 3-d model does accurately predict the wake shape and deficit downstream of the rotor despite not modelling the boundary layer in the vertical.

In the GH far wake report (Thomson, *et al*, 2011c) it was noted that the far wake width and height of the Gaussian profile may be distorted by the bounding effects of the free-surface and the seabed. This is investigated in Table 5 where the wake width and height has been calculated for test 13 at all downstream positions where measured flow traverses have been taken. It is suggested that, if the results for the central rotor were neglected then the data suggests that the wake width and height are not comparable for a duration between 4D and 10D. The reason that the central rotor should be neglected is because, when fitting the Gaussian curve we obtain poor results as the deficit in the lateral direction is `flat' in this region producing a large standard deviation in the lateral direction.

From the assumptions that were discussed in section 5.1 it is not surprising that the 3-d model performs better with respect to mixing in the lateral and vertical directions. The model accounts for the wake mixing and merging of multiple wakes. In comparison, the 2-d model blends multiple wake deficits together using averaging techniques and consequently does not recreate the flow downstream of the rotors as well. Instead the tendency is to predict multiple peaks and troughs rather than mix the fluid evenly as one would expect to occur in a turbulent flow.

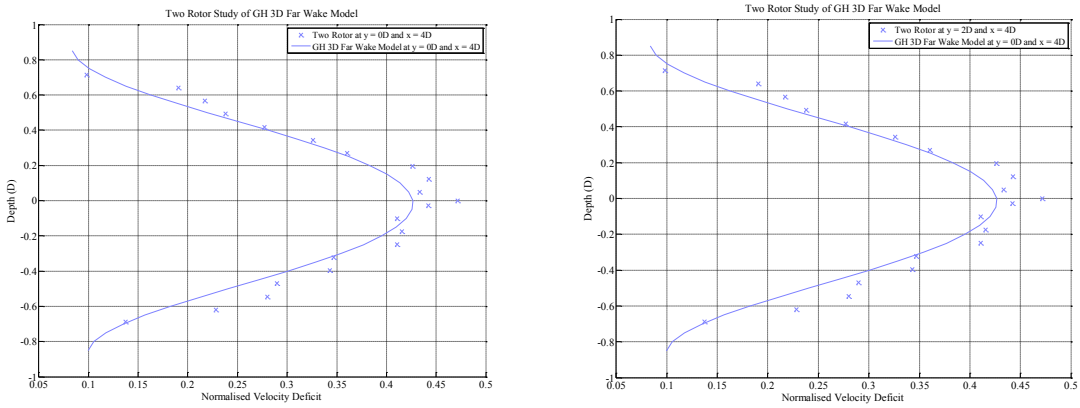

Figure 5-9: Comparison of the velocity deficit in the vertical from test 07 at $\boldsymbol{y = 0D}$ for the GH 3-d wake model.

Given that turbines are often placed in a staggered formation (Bai *et al*,2009) to aid energy production and wake recovery, it is important that the velocity between rotors is predicted accurately. This gives the 3-d wake model a clear advantage over other 2-d models which only predict the centreline velocity deficit due to one independent turbine.

5.4 Conclusions and further work

The 2-d and 3-d models have been compared to data from multiple rotor experiments performed in Thomson *et al* (2011a). The centreline velocity deficit agreement has been found to be very good provided the correct starting point for the wake model is chosen correctly. The wake start point has been quantified through a sensitivity analysis where error has been minimised. In addition, the wake width and shape was correctly predicted giving confidence that the set of equations and turbulence closure model are sufficient to model the wake of a turbine.

In addition, a sensitivity analysis of the ambient turbulence input parameter was performed by comparison to the experimental data sets. Given that the turbulence intensity dropped in the flume from 10% to 8% it was found that varying the value of this parameter still gives good agreement with the experimental measurements and affects the flow in the predicted fashion. From test 07 it was seen that the velocity deficit was over-predicted passed 4D downstream. In test 13, 8% turbulence intensity produced good results with the measured data.

The effects of wake merging have also been investigated by comparison to the 2-d and 3-d models. The agreement between the 3-d model and the measurements is very good, while the 2-d model under-predicts the velocity deficit between two adjacent rotors. In comparison, the wake merging algorithms produce reasonable results.

How the wake width and shape was affected by the bounded nature of the flow was explored. It was found that the shape cannot necessarily be assumed to be circular and that the wake may be squashed. However, more experimental data would be required before we could form firm conclusions. What is clear, however, is that the 3-d wake model appears to give excellent results with respect to lateral and vertical measured data even at 12 D downstream of the rotor plane - this is an encouraging result.

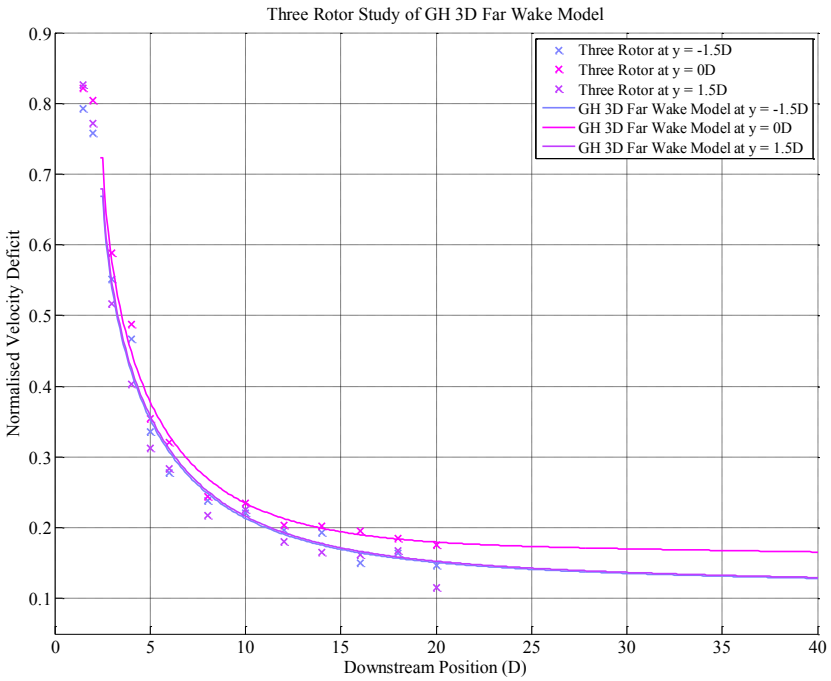

Figure 5-10: Results of 3-d wake model against experimental results for three rotors at 1.5D lateral separation in test 13.

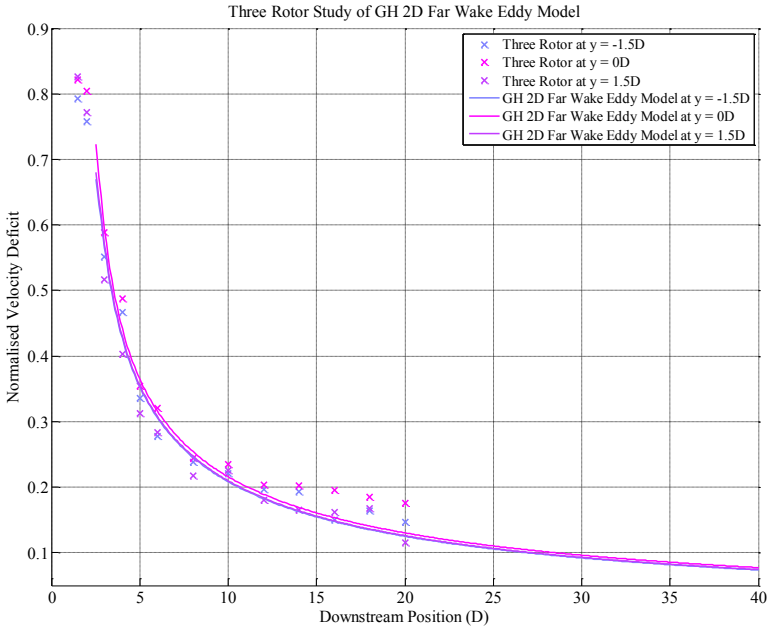

Figure 5-11: Results of 2-d comparison against experimental results for three rotors at 1.5D lateral separation in test 13.

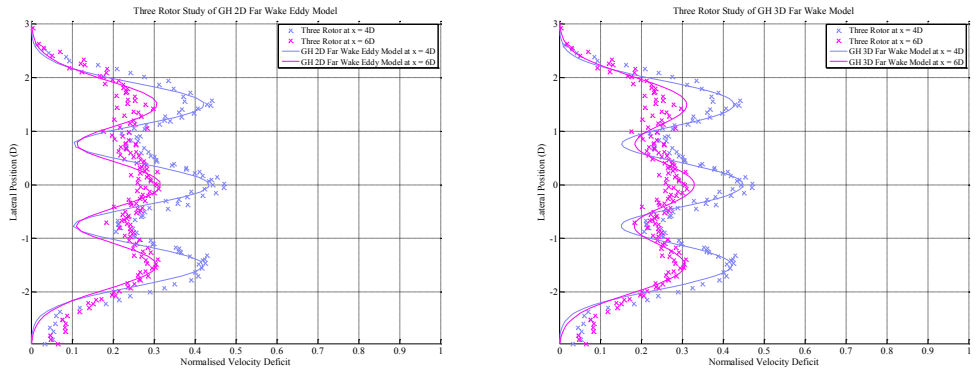

Figure 5-12: Lateral velocity deficits form test 13 of the 2-d with wakes merged using a root mean square algorithm and 3-d wake models at 4D and 6D downstream of the rotors.

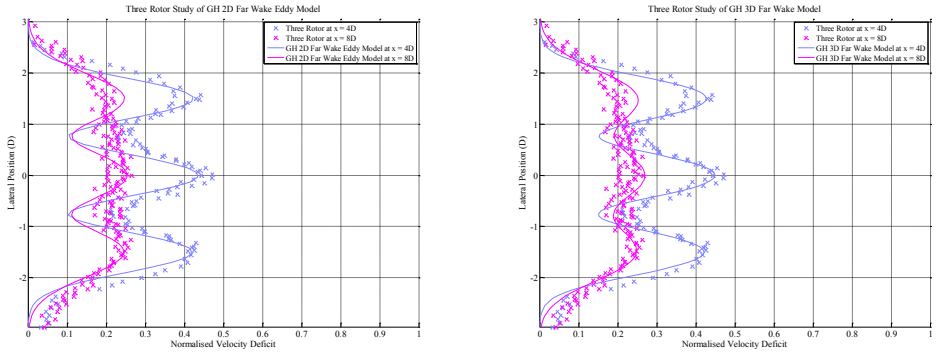

Figure 5-13: Lateral velocity deficits from test 13 of the 2-d with wakes merged using a root mean square algorithm and 3-d wake models at 4D and 8D downstream of the rotors.

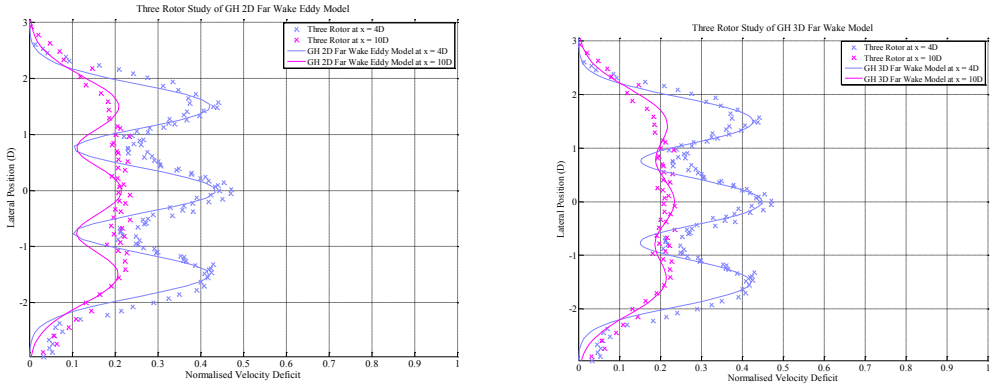

Figure 5-14: Lateral velocity deficits form test 13 of the 2-d with wakes merged using a root mean square algorithm and 3-d wake models at 4D and 10D downstream of the rotors.

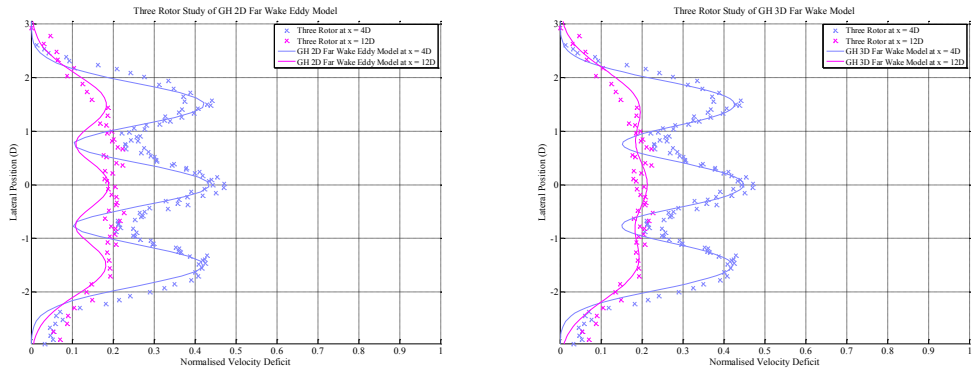

Figure 5-15: Lateral velocity deficits from test 13 of the 2-d with wakes merged using a root mean square algorithm and 3-d wake models at 4D and 12D downstream of the rotors.

A comparison with the remaining experimental tests performed in WG4 WP2 should be performed. This includes modelling the added turbulence intensity and also producing an error analysis to measure the uncertainty in model predictions. Eventually, measured data error will also be incorporated to quantify the aggregated uncertainty in the far wake model.

While initial results are encouraging, the model has still not been proven to model multiple rows of devices. In addition, the experiments in WG4 WP2 will only validate the model for a small range of thrust operating points and ambient turbulence intensity. More tests that are required include experiments performed at different thrust coefficients and different turbulence intensities. These will give more confidence that the wake deficit predicted by the two models is adequate in describing inter-array effect when turbines are extracting energy from a tidal flow (Duckworth & Barthelmie, 2008). Results from WG4 WP1 and WG4 WP3 will help validate the far wake model for a variety of different operating and environmental conditions. In addition, the results from WG4 WP3 will also test different vertical blockage ratios.

Table 4**:** Sensitivity study of the distance downstream of the rotor defined as the start of the wake on the uncertainty of the Eddy2D and Eddy3D Far Wake Model (FWM) for WG4 WP2 (UoM) Test 05. Values for the total, maximum and average error are provided.

		Eddy 2D FWM Model Uncertainty								
Wake start position (Diameters downstream)	Ct	Centerline			Lateral			Vertical		
		Tot.	Max.	Avg.	Tot.	Max.	Avg.	Tot.	Max.	Avg.
1.5	1.045	169.02	41.32	13.00	4390.28	133.47	71.97	3580.63	135.68	102.30
2.0	1.038	71.09	18.14	5.92	4074.75	162.09	66.80	3166.83	121.89	90.48
2.5	0.932	39.54	10.08	3.59	4804.02	301.69	78.75	3148.33	123.21	89.95
3.0	0.786	81.33	19.28	8.13	8080.48	748.25	132.47	3409.39	134.31	97.41
3.5	0.680	131.76	28.05	13.18	14379.7	1754.35	235.73	3765.04	153.28	107.57
4.0	0.575	198.15	40.56	22.02	n/a	n/a	n/a	n/a	n/a	n/a
4.5	0.528	218.27	46.11	24.25	n/a	n/a	n/a	n/a	n/a	n/a
5.0	0.482	243.99	53.05	30.50	n/a	n/a	n/a	n/a	n/a	n/a

		Eddy 3D FWM Model Uncertainty								
Wake start position (Diameters downstream)	Ct	Centerline			Lateral			Vertical		
		Tot.	Max.	Avg.	Tot.	Max.	Avg.	Tot.	Max.	Avg.
1.5	1.045	147.05	38.01	12.25	3574.14	114.22	58.59	2767.42	117.33	79.07
2.0	1.038	115.73	19.35	9.64	3196.33	105.96	52.40	2417.75	100.78	69.08
2.5	0.932	24.61	8.76	2.05	3777.43	239.57	61.93	2625.66	103.55	75.02
3.0	0.786	150.90	23.65	13.72	6815.25	604.56	111.73	3310.95	128.87	94.60
3.5	0.680	276.88	43.90	27.69	12343.7	1403.20	202.36	3918.57	152.51	111.96
4.0	0.575	443.67	71.05	44.37	26690.0	3912.08	437.54	4943.83	227.17	141.25
4.5	0.528	497.77	84.14	55.31	32075.6	4727.53	525.83	5876.97	269.26	167.91
5.0	0.482	558.84	99.47	62.09	38427.9	5687.17	629.97	6996.63	319.08	199.90

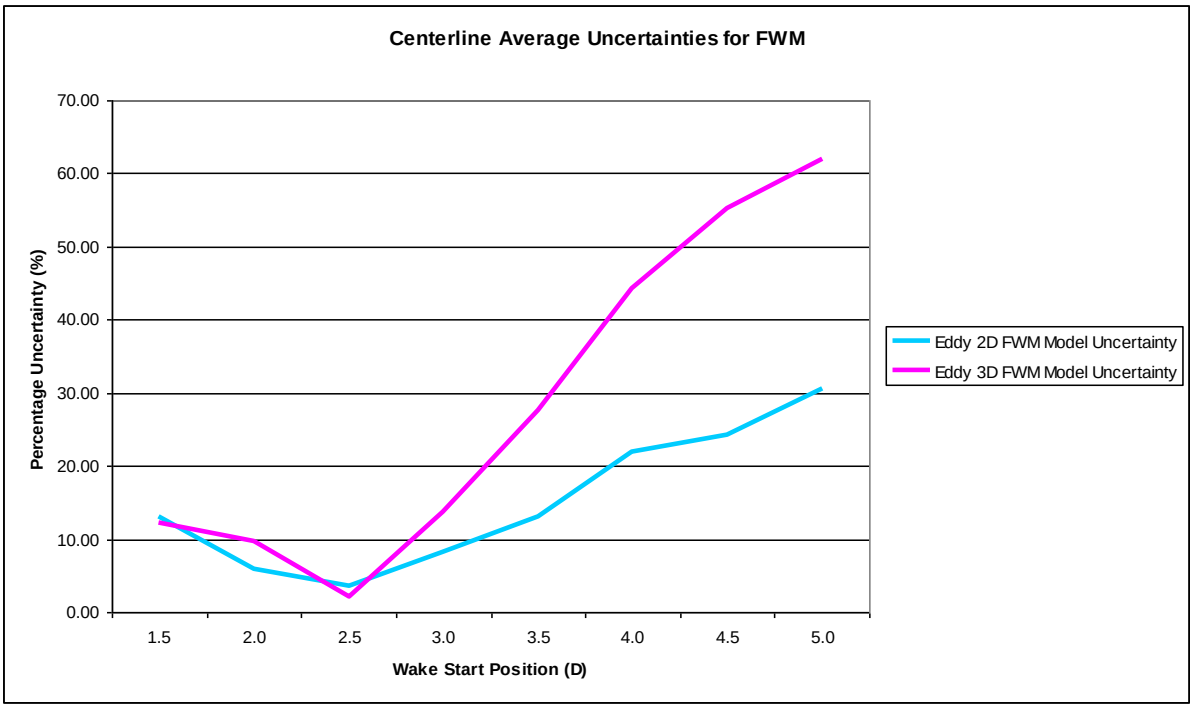

Figure 5-16: Effect of the wake starting position on the error for the Eddy 2D and Eddy 3D GH Far Wake Model for WG4 WP2 (UoM) Test 05.

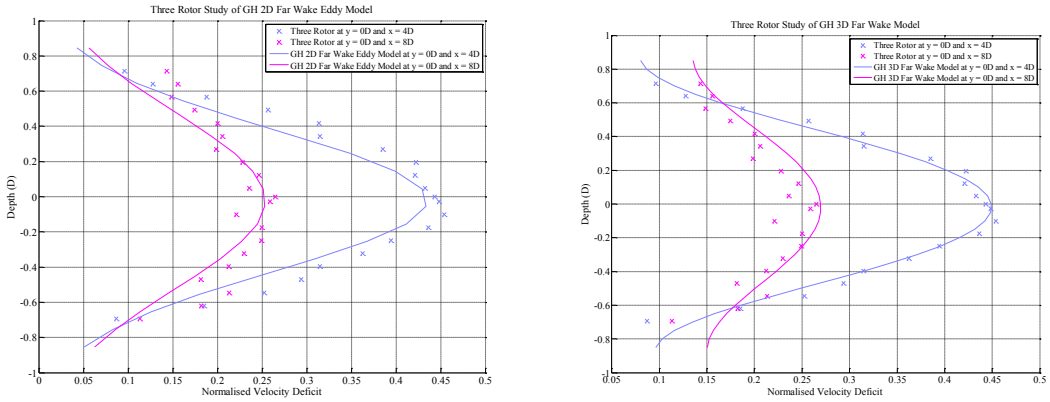

Figure 5-17: Vertical velocity deficits from test 13 showing the 2-d (with wakes merged using a root mean square algorithm) and 3-d wake models at 4D and 8D downstream of the central rotor (y=0D) for WG4 WP2 (UoM) Test 13.

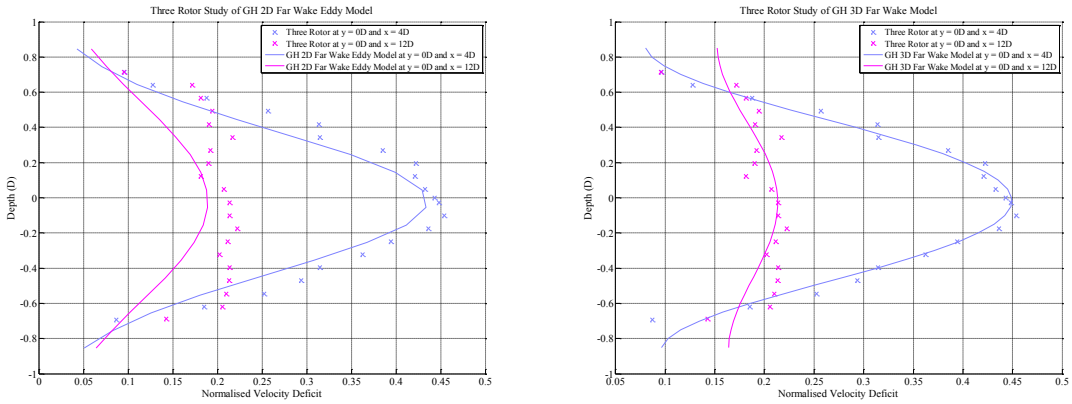

Figure 5-18: Vertical velocity deficits from test 13 showing the 2-d (with wakes merged using a root mean square algorithm) and 3-d wake models at 4D and 12D downstream of the central rotor (y=0D) for WG4 WP2 (UoM) Test 13.

Table 5: Changing of peak normalised velocity deficit wake width with downstream distance for WG4 WP2 (UoM) Test 13.

	Peak 2D Normalised Deficit					
Lateral Rotor Pos (D)	Distance Downstream					
	x = 2D	x = 4D	x = 6D	x = 8D	x = 10D	x = 12D
-1.5	0.84	0.43	0.29	0.24	0.23	0.21
0.0	0.85	0.44	0.28	0.23	0.22	0.31
1.5	0.82	0.41	0.25	0.21	0.21	0.20

	Wake Width (Sy)					
Lateral Rotor Pos (D)	Distance Downstream					
	x = 2D	x = 4D	x = 6D	x = 8D	x = 10D	x = 12D
-1.5	0.36	0.56	0.73	0.81	0.85	1.15
0.0	0.35	0.58	1.00	1.74	2.75	50.50
1.5	0.35	0.59	0.84	1.15	1.14	1.02

	Wake Height (Sz)					
Lateral Rotor Pos (D)	Distance Downstream					
	x = 2D	x = 4D	x = 6D	x = 8D	x = 10D	x = 12D
-1.5	0.33	0.44	0.59	0.71	0.84	1.35
0.0	0.34	0.45	0.58	0.74	0.94	1.08
1.5	0.34	0.47	0.58	0.59	0.88	1.15

6 FLOW FIELD MODEL

In this section we will review the work currently undertaken by GH to assess the performance of the flow field modelling algorithm adopted in TidalFarmer. In order to calculate the flow field, of a tidal cycle, GH believe that existing hydrodynamic models such as Telemac and Mike 21 DHI 2012 (Thomson & Gill, 2011b) should be used to calculate the 2-d depth-averaged flow field. However, in order to accurately predict the expected energy yield, the 3-d flow field must be known. However, calculating a 3-d flow field is more computationally expensive. Therefore, GH propose extrapolating to 3-d by assuming that the velocity profile through the water column follows a power law profile. The objective of this chapter is to discuss the validity of such an approach by comparison to both numerical and experimental work.

The power law profile is derived from a classical solution to turbulent flow along a flat plate (Schlichting, 2000). This solution for the velocity profile will be compared against three independent free-surface experiments. Two experiments focus on flow acceleration and deceleration which occur due to flow moving over a ridge like bathymetry feature (referred to in the literature as a sill) (Blom,1995). The results from another experiment observe flow acceleration due to some foundation structure placed on a seabed to accelerate the flow for tidal energy extraction (Giles *et al*, 2011).

It is noted in Giles *et al*, (2011) and Garrett & Cummins (2005) that ideally the flow will be fast flowing and the velocity profile would be uniform to maximise power generation and minimise unequal loading on the blades. If these conditions are satisfied then tidal turbines should be placed in regions where the flow is being accelerated and not decelerated. In this case, it will be shown that the power law predictions yield good results, given the GH philosophy and objectives of the model.

6.1 Background of flow model

In Thomson, *et al* (2011a) the following assumptions were made in order to model the flow velocity in the vertical:

- Steady flow – The model is assumed to be time independent.
- Turbulent flow – The Reynolds number of tidal flow is large given the small kinematic viscosity of sea water (Salmon, 1998). Therefore, the flow is turbulent.
- Incompressible – Variation in the fluid density is supposed to be small. The primary cause of density fluctuation in ocean circulation models is due to temperature and salinity gradients (Salmon, 1998). It is assumed that these are unimportant in comparison to the magnitude of convection, shear stress and pressure gradients.
- Shallowness/Hydrostasis – The flow is assumed to be shallow such that the vertical velocity is small and the pressure in the vertical is hydrostatic.
- Fully-developed flow – In this case, a flow is fully-developed when turbulent drag balances with the driving pressure gradient. The analogue is a Poiseuille flow in a laminar flow regime (Anderson, 1995).

In order to extrapolate a 2-d depth-averaged flow to a 3-d flow it is proposed that a power law profile is used to determine the vertical velocity profile.

The model takes input parameters for the seabed surface roughness that can then predict the shape of the velocity profile in the vertical. Therefore, given a surface roughness value $k_s$the Darcy friction function f can be calculated using

$$\left(\frac{1}{\mathrm{f}}\right)^{1/2} = 2\log_{10}\left(\frac{\mathrm{D_h}}{\mathrm{k_s}}\right) + 1.14,$$

where $\mathrm{D_h}$is the hydraulic diameter (Chanson, 2004). The power law is determined via the equation

$$\mathrm{N} = \mathrm{K}\left(\frac{8}{\mathrm{f}}\right)^{0.5},$$

In order to obtain the horizontal velocity through the water column in a free-surface flow of depth $H$with friction velocity $\mathrm{u_h}$ we use the equation (Pope 2010),

$$\frac{U}{u_h} = \left(\frac{z}{H}\right)^N.$$

The shallow water equations are derived under the assumption that horizontal length scales of the flow are typically much greater than vertical scales (Salmon, 1998). The implication of this assumption is that the magnitude of the vertical velocity is always much smaller than that of the horizontal. This can be seen through a scaling argument of the continuity equation. In the shallow fluid paradigm, the pressure is quasi-hydrostatic such that the only transfer of momentum in the vertical is due to the weight of the water pressing down upon itself.

As a consequence of the assumption of hydro-stasis, the equations give poor predictions when trying to model flow over steep bathymetry gradients. This is because the assumption of shallowness, i.e. large longitudinal length, compared to small height, are broken. An example of phenomena that will be poorly predicted is flow separation, whereby the flow reverses direction. This typically occurs for a hydraulic flow over a backwards step (Bravo *et al*, 2000). Near an area of recirculation, the vertical and horizontal velocities are comparable in magnitude such that the assumption of shallowness is violated.

The logarithmic and power law profiles are standard descriptions of a fully-developed boundary layer flow over a flat, rough surface (Tennekes & Lumley, 1972). The logarithmic velocity profile is derived assuming there exists a pressure–drag balance similar to a laminar Pouseillie flow described in Anderson (1995). This approach was adopted in Dyer & Soulsby (1988) where a logarithmic profile was obtained as a solution to a simplified system of equations given a parabolic mixing profile for the Reynolds shear stress. Hence, for an idealised flow geometry and a simple equilibrium between the pressure and drag, the velocity can be accurately predicted. It has also been shown that a power law profile also gives a suitable description of the flow field (Pope, 2010).

As a first approximation, the logarithmic profile has been successfully applied to wind flow over varying topography (Jackson & Hunt, 1975) and in free-surface flow over varying bathymetry (Blom & Booij, 1995). Typically, correction terms are then added to the logarithmic profile to model the flow acceleration and deceleration that occur when the flow moves over terrain of varying height. In these cases, the assumption that the bathymetry gradients are small is critical so that the perturbations to the zeroth-order logarithmic solution can be calculated.

In flow over varying surface topography, for example Jackson & Hunt (1975), it was discovered that as the flow accelerates there is an inter-play between the inertia, pressure and drag of the flow. A similar dynamic balance exists in free-surface flow over a ridge (Blom, 1995). As the flow moves over a bathymetry feature the flow is no longer hydrostatic. In fact, when accelerating up the ridge the drag increases (pressure-drag balance), on a downwards slope of the hill the flow decelerates and there is an

inertia-drag balance. Generally speaking, the power law model gives a reasonable fit if the flow is accelerating as it is derived under the assumption of a pressure-drag balance.

As will be shown, the model gives good results provided the bathymetry is flat, as predicted. However, for flow over varying bathymetry, the model performs poorly in regions of deceleration. It is also noted that, the next level of modelling – solving the shallow water equations using a numerical method such as a pseudospectral method (Trefethen, 2000) - does not significantly improve the results.

6.2 Description of validation methodology

At present, velocity profile measurements of tidal flow have been restricted to data taken at ADCPs in scattered locations throughout a tidal site. The actual velocity profiles of tidal flow over some underwater obstacle, such as a ridge are not commonplace. However, there are experimental and numerical studies that have examined the flow over varying bathymetry.

In order to assess the limitations of the GH model the following studies should be performed. First, a rigorous comparison of measurements taken for a flow over some underwater obstacle should be made. The primary interest is how well the power law profile will fit with the velocity profiles for flow moving over an obstacle. To form a comparison, a variety of investigations which examine different bathymetry gradients will be performed. The Froude number will be comparable with a value for tidal energy extraction which is approximately Fr = 0.1 (Thomson *et al*, 2010c).

Further studies will be made against the measurements of coastal basin flow taken as part of the ReDAPT project. This will allow a test of the combined 2-d shallow water model employed by GH, coupled with the power law extrapolation of the GH flow field. In addition, there will be an opportunity to compare the GH model against a 3-d model of the Fall of Warness. This will allow us to assess the capability of the model in comparison to more computationally expensive techniques.

6.3 Model validation and verification

The GH flow model is compared to the results of two independent experimental studies and one numerical study.

6.3.1 Numerical free-surface flow

A verification with ROMS (Arango & Shchepetkin, 2012) has been performed in order to draw a comparison with numerical simulations, using well-established software. ROMS is a free-surface, terrain following, primitive equations ocean model widely used by the scientific community for a diverse number of applications, see, Song & Haidvogel (1994). It has been thoroughly developed and tested and is an open source code for which there exists an extensive online literature.

The computational domain was defined as follows, x direction is the streamwise, y is the cross stream and z the vertical direction. The values for the horizontal domain were (x,y) = [0,1000] x [0,1000]. A slip boundary condition was used at y = 0 and y = 1000 m. The hill in the ROMS simulation was modelled as a three-dimensional ridge as shown in Figure 6-1 for which the shape parameters were chosen to be ζ = 350 m, λ = 100 m, δ = 10 m and μ = 100 m. The velocity and free-surface profiles were taken along the line y = 500 m taking a cross-sectional slice of the flow.

The ROMS simulation was computed in a 3-d flow field. The Coriolis force, density fluctuations due to temperature and salt concentration were neglected and forcing was set to zero. The steady state flow over a ridge was calculated. A quadratic bottom friction was used in order to model the seabed shear and the roughness length chosen was z0 = 0.002 m. A no-slip condition was applied at the seabed and

no-shear was applied at the sea surface. The turbulence closure model used to close the system of equations was the k-ε turbulence closure model (Durski *et al*,1994). The inflow height was h0 = 20 m and the flux per unit width was specified to be q=13 sq m/s. Hence the Froude number at the inflow boundary was Fr = 0.046.

Table 6: Summary of investigations of free-surface flow over bathymetry. The inflow flux, height and geometry of the ridge are recorded for each experiment.

Test	Flux	Height	Fr	ζ	μ	δ	λ	Slope
ROMS	13.0	20.0	0.046	350	100	10	100	1/10
Blom	0.4	0.16	0.17	0.5	0.6	0.08	0.4	2/15
Giles	0.1284	0.30	0.25	0.3	0.05196	0.03	0.4	3/40

The results of a simulation performed using ROMS for the geometry and inflow values described in Table 6 are presented in Figure 6-2. We can see that the power law profile gives good agreement to the ROMS results in Figure 6-12 (a-d) and (h-i). As expected, the model predicts flow over a flat surface or in the acceleration zones. However, the power law profile does not predict the more uniform flow profile which is associated with flow acceleration. In addition, the worst agreement of the power law profile is when the flow decelerates on the downstream face of the ridge. In comparison, the numerical solution of the SWE equations gives a reasonable fit of the numerical data. Therefore, there is some advantage to solving a simplified system of equations as the flow in the deceleration zone is well predicted.

6.3.2 Experimental free-surface flow

The next measured data set we shall compare with is the work undertaken by Blom (1995). The purpose of this study was to improve the calculation of the velocity field for flow over a submerged dam. This included calculating the velocity profile through the water column using a modified set of shallow water equations. The results were then validated against experimental work and verified against a Navier-Stokes numerical solution.

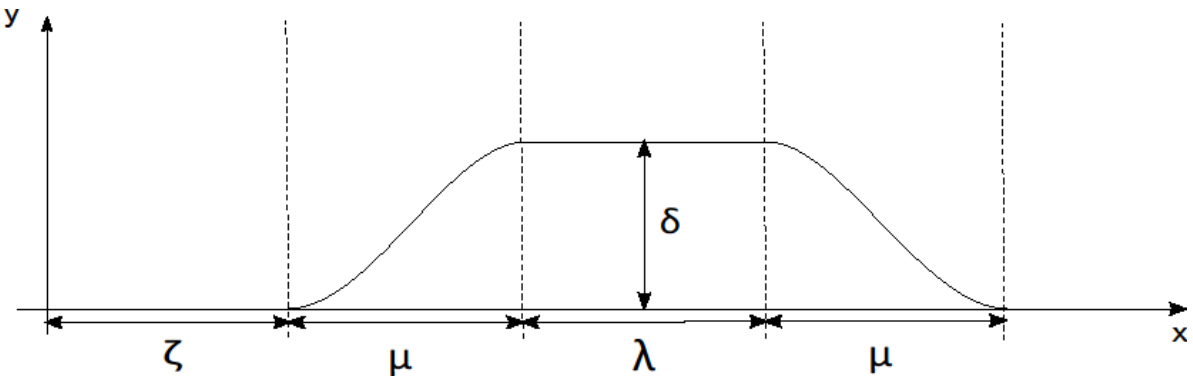

Figure 6-1: Generic ridge like feature used for computations of free-surface flow field.

The results are presented in Figure 6-3. It is worth noting that there are four distinct regions – equilibrium, acceleration, deceleration and recovery. Once again the power law profile gives a good description of the flow in regions of equilibrium (flat surfaces) (a-b) and (i), away from regions where the flow is accelerating and decelerating (upstream and downstream faces of the ridge). On the crown of the ridge we can see that from the experimental results in (c) and (d) the flow is recovering. Whereas the flow profile in (c) is uniform, the profile in (d) has more pronounced shear by comparison. This is because turbulence acts to redistribute the momentum. In the deceleration zone (e-f), the power law gives very poor results as does the pseudo-spectral solution to the SWE.

A discrepancy in flux conservation appears to occur in (c). However, this is caused by the free-surface dip that occurs when subcritical flow moves over a hill (Paterson, 1983) which is exaggerated by the high Froude number of this flow study. A second region of flow recovery occurs downstream of the ridge in figures (g-i). The pseudo-spectral model predicts the recovery reasonably well. However, the power law fit is reasonable only in profiles (h-i).

6.4 Comparison against numerical simulations

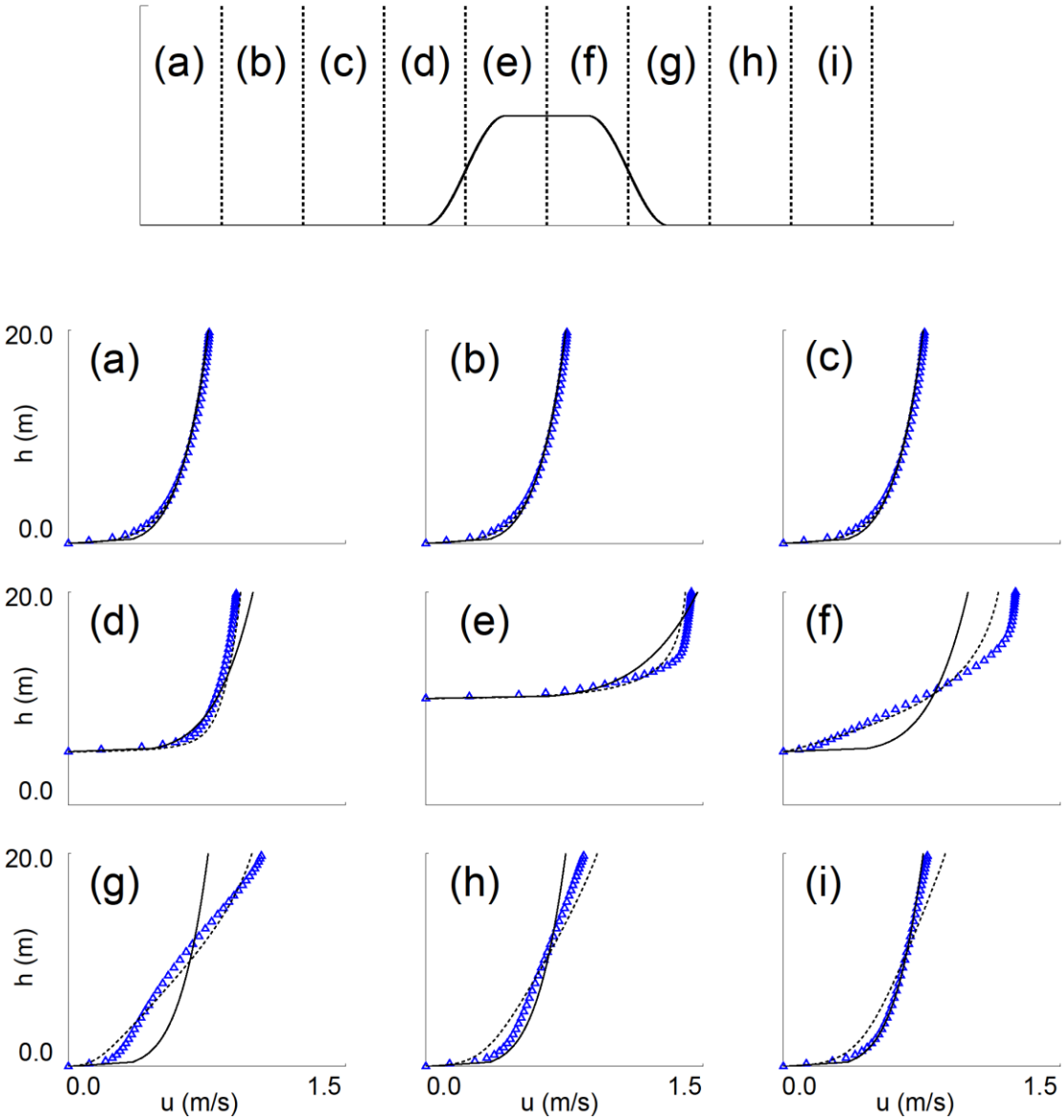

Figure 6-2: Results of ROMS simulations (Δ) against GH power law model (-----) and pseudo-spectral solution to the shallow water equations (- - -) for flow over a ridge for $\mathbf{k_s = 55.24}$.

It was decided that free-surface deformation is simply a local effect and therefore would have little importance in tidal energy extraction (Thomson, *et al* 2011). It is clear from these results that, if the free-surface deformation is significant then this would have an impact on the accuracy of the power law profiles determined using the GH model. Therefore, it is important to understand how important this factor is in regions where tidal turbines will be placed. Only by comparison to measured ADP data and hydrodynamic models through the ReDAPT project will we be able to quantify this uncertainty.

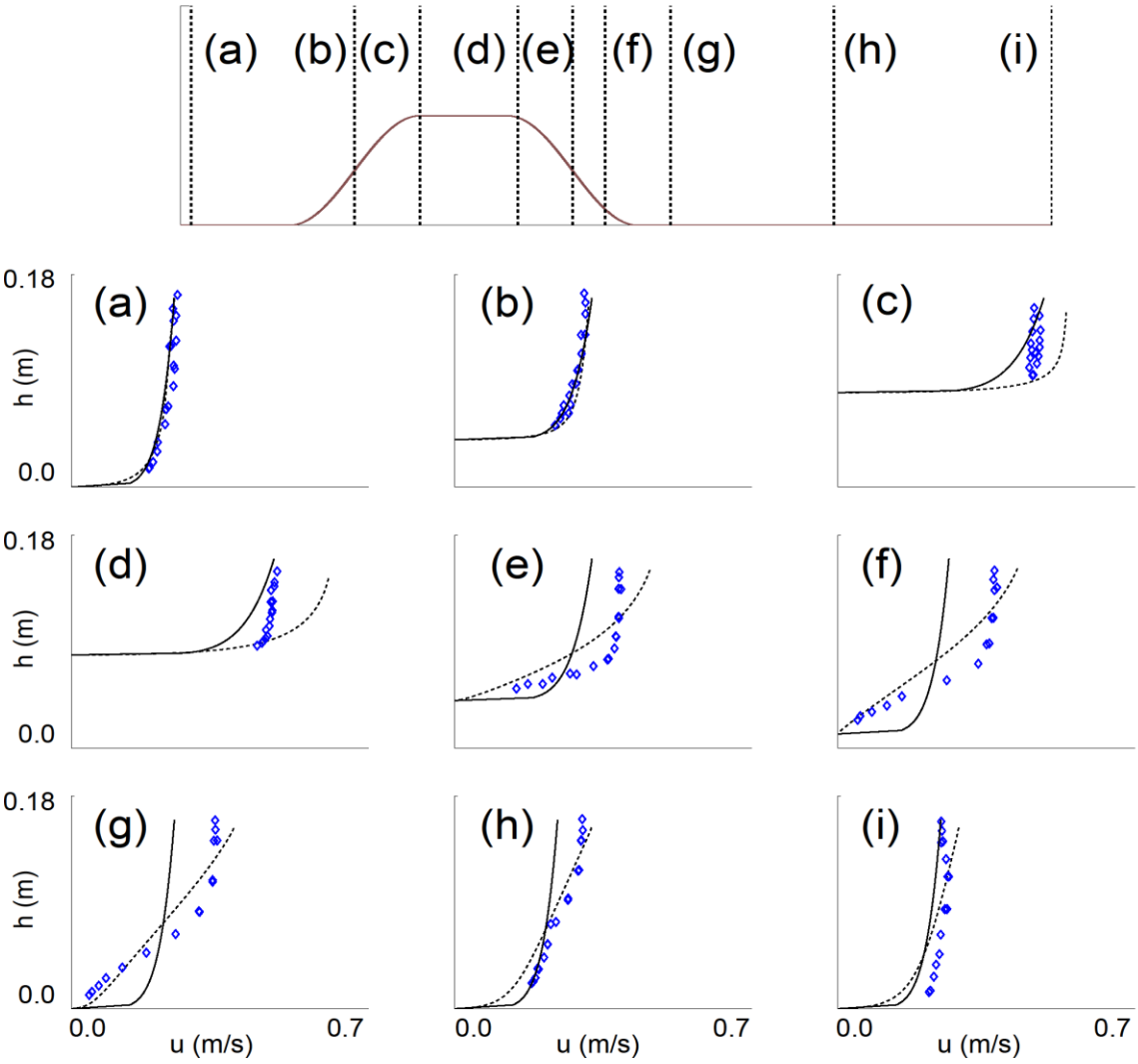

Figure 6-3: Experimental measurements (◊) of flow over a ridge compared to the GH power law model profile (-----) and a numerical solution to the shallow water equations (- - -). This was calculated using a roughness value of $\mathbf{k_s = 0.4169}$.

A final comparison has been drawn against Giles *et al*, (2011) where flow acceleration due to a foundation ramp was investigated. No flow measurements were taken on the downstream face of the ridge. Again it is clear to see from Figure 6-4, that while the flow along a flat-surface can be well predicted, the acceleration of free-surface flow is not so well captured.

Table 7 gives a summary of the average error throughout different points in the flume for the experiments and numerical simulation comparisons. These results are in line with our earlier comments and allow the error to be quantified. It is plain to see that when the flow is in equilibrium the GH model is to within 10 % of measurements, while for accelerating flow the error is never greater than 20%. In the deceleration zones the error is high, being over 40%.

6.5 Conclusions

A review of the underlying assumptions of the model is provided:

- Steady - This is well satisfied given the low frequency of the tidal cycle.
- Turbulent flow - The assumption of turbulent flow is justified as the GH model predictions perform well in comparison to the experimental data in regions where the seabed is flat.
- Incompressibility – This is a standard assumption for modelling hydrodynamic flows and is justified given the results for the model predictions.
- Fully-developed - It has been found that the error is lowest when the bathymetry is flat. This is because the power law profile is derived under the assumption that the flow is fully developed. Provided the bathymetry is flat at a tidal site, we can have confidence that the model will predict the results with a good level of accuracy (to within 20%).
- Hydrostasis - The largest errors indeed occur when the flow is accelerating and decelerating. This is because the pressure drag balance which was assumed to exist is no-longer valid given that the flow is non hydrostatic. Any changes in local bathymetry will violate this condition. For wind flow over varying topography even very small deviations away from zero gradient cause changes in the flow away from the power law profile (Jackson & Hunt, 1975).

The power law described in Thomson (2011b) has been applied to three independent studies. In each case the power law profile performs as expected. The flow along a flat-surface is reproduced well but is poor when the flow accelerates or decelerates. However, the discrepancies between measured data or numerical models does not differ markedly from the power law prediction, in the acceleration zone. It is noted that the model gives better predictions when the bathymetry gradient is small. In particular the error is around 4 % when compared to measurements from (Giles *et al*, 2011) for flow over a ridge with a maximum slope of 3/40. It is therefore recommended that the model only be used to accurately predict flow for these gradients and that serious errors can occur if the gradient is larger.

If it is found that the power law fit is not adequate to describe the flow at a real tidal site, through comparison to data provided in the ReDAPT project, then we may consider two alternative options. The GH model may be replaced by either; a solution to the 2-d shallow water equations, such as shown in Figure 6-2 and Figure 6-3, or even a 3-d hydrodynamic model. Similar work, in this field, has been undertaken in the ReDAPT project where a Mike3 hydrodynamic model has been constructed to model the Fall of Warness (Gunn & Stock-Williams, 2012). In this report, the 2-d depth-averaged flow was recreated with a high level of accuracy. However, it was found that the sometimes, the depth velocity profiles were not always predicted correctly. It is clear that a greater understanding of how to model and calibrate hydrodynamic flows is required for a good level of accuracy to be achieved.

In conclusion, the GH model serves as a useful tool which will be able to predict the speed ups of tidal flow with a reasonable level of accuracy (to within 20 %) and low computational cost. It is anticipated that tidal turbines will be placed in regions where the velocity profile is uniform and the flow is fast such as over flat regions of bathymetry or in an acceleration zone (Giles *et al*, 2011, Garrett & Cummins, 2005). Therefore, at present the GH model appears to be adequate in predicting the vertical flow velocity.

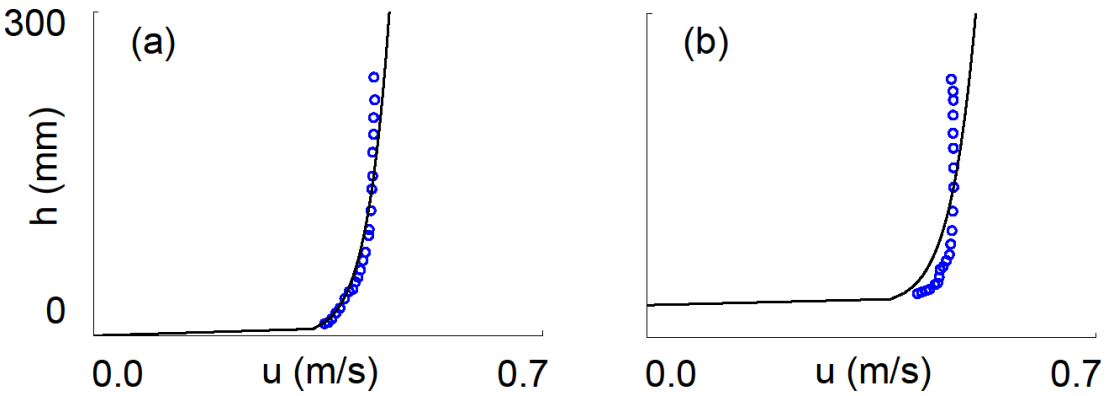

Figure 6-4: Experimental measurements (○) of flow over a ridge compared to the GH power law model profile (-----). This was calculated using a roughness length of $\mathbf{k_s = 0.8848}$.

Table 7: Summary of the average error, calculated using equation 2, between GH model predictions using the power law and the experimental and numerical results discussed in section 6.3.

Data set	(a)	(b)	(c)	(d)	(e)	(f)	(g)	(h)	(i)
Blom	4 %	2 %	8 %	13 %	25 %	47 %	44 %	12 %	14 %
ROMS	7 %	7 %	7 %	18 %	11 %	29 %	29 %	19 %	14 %
Giles	1 %	4 %	-	-	-	-	-	-	-

7 SUMMARY AND FURTHER WORK

The GH blockage, flow field, near wake and far wake models have been compared to measured data made available through the PerAWaT project. For the range of physical parameters that we wish to test, the results are very encouraging. At the present time an initial errors analysis of the individual models has been undertaken. The uncertainties across the various models range between 1-10% and in some atypical cases up to 20 %.

At this stage the combined effect of the uncertainties has not been evaluated at this point. This will be undertake in D19 once all the models have been developed further and validated.

The next steps are to continue processing the remaining data sets being made available and to begin a thorough uncertainty analysis that takes into account GH model and measurement errors. Once the limitations are known between experimental and GH model predictions an aggregate analysis can be undertaken. This will allow us to estimate the accuracy of energy yield predictions.

Table 8 provides a summary of the progress made on analysing all data sets available for model validation. In addition, the next steps and challenges that remain are discussed.

Table 8: Summary of current status of PerAWAT work packages, and challenges in model validation and next steps.

Work package	Status	Next steps, challenges
WG3 WP1 D4	Results are being uploaded – **Critical path dependency.**	• Analyse blade resolved simulations. Determine velocity deficit and wake width by fitting Gaussian curve. • Compare results with those from WG4 WP1, WG4 WP2 and eventually WG4 WP3 for similar operating values of Ct to measure confidence in numerical predictions. This will inform us of how reliable the numerical simulations are for comparison to the GH near wake model. • Perform analysis with GH near wake model. • If GH near wake model not sufficiently accurate, consider different parameterisations (perhaps using WG3 WP5 work). • GH near wake model uncertainty analysis to be estimated. • Consider next steps, e.g. what will the impact of waves be, are there further simulations that would be of interest to help model verification. • Workshop, where LES is compared to Fluent simulations using RANS for a greater understanding of results and there applicability D20 (under variation).
WG3 WP2	-	• At present, it is the belief of GH that the results are not sufficiently accurate with comparison to measured data (WG4 WP2) to warrant a comparison with the GH far wake model. • The processing of this data will not be considered for the time being given that the continued value of this project is in doubt.
WG3 WP3 D3	Due March 2013 – **Critical path**	• Energy extraction tool has been developed such that the input of results from WG3 WP3 D1 can be loaded for a comparison between Telemac and TidalFarmer. • Device layouts have been agreed with Tom Adcock and Vanessa Martin.

Work package	Status	Next steps, challenges
	dependency.	• Points for measurement comparisons between the respective models have been specified. • The times for which the tidal flow simulations should be run have been specified. • Obtain bathymetry data for the site through GEBCO website. • Run TidalFarmer simulations to compare against Telemac model. • Perform uncertainty analysis at pre-specified points.
WG3 WP5	Due November 2012 - **Critical path dependency.**	• Gain knowledge of parameterisation developed under WG3 WP5 D3. • Obtain data from WG3 WP5 D1 & D2 and compare to GH near wake model. This will be provided inWG3 WP5 D3. • Include this data in uncertainty analysis for the GH near wake model. • Obtain near wake flow results for high and low-solidity devices. • Use near wake data to fit to Gaussian curve and compute wake width and velocity deficit. • Assess value of data by comparison to WG4 WP1, WG4 WP2, and WG4 WP3 results at equivalent operating points. • Perform analysis using GH near wake model. • Perform analysis on Near wake data using parameterisation developed under WG3 WP5. • Measure model uncertainty be calculating the error. • Workshop, where code-Saturne RANS results are compared to LES for a greater understanding of limitation and value of data set.
WG4 WP1	Delivery complete.	• High blockage ratio means that any comparison formed needs careful consideration. • Data processing complete. • Fit GH Gaussian curve to near wake profiles undertaken. • Assess value of data set with comparison to WG4 WP2 and WG4 WP3 data set. • Form a comparison with the GH near wake model. • Measure the model error and measurement error in order to form uncertainty analysis. • Run the blockage model and compare to experimental results. • Measure the model error.
WG4 WP2	Delivery complete - **Critical path dependency.**	• A study on the best wake merging algorithm to impose the deficit from the second row of turbines needs to be undertaken for the GH far wake model. • Complete comparison study of GH far wake model against measured results for multiple rows. • Assess performance of current GH near wake model by comparison to collated near wake data. • Compare measured turbulence intensity with GH added turbulence intensity model. • Make modifications to added turbulence model if required. • Model validation to be performed using the blockage model for different array layouts. • Uncertainty analysis on model predictions for the GH blockage,

Work package	Status	Next steps, challenges
		near wake and far wake against the measured data. • Consider aggregate uncertainties.
WG4 WP3	Experiments delivered end of November 2012.	• The experimental results will not be fully available until the end of November 2012. • Process incoming data sets as they arrive. • Determine velocity deficit and wake width by fitting Gaussian curve to the near wake. • Compare results with those from WG4 WP2 for similar operating values of Ct to measure confidence in experimental measurements. • Perform analysis with GH near wake model. • Perform analysis with GH blockage model. • If GH near wake model not sufficiently accurate, consider different parameterisations (perhaps using WG3 WP5 work or modifying existing GH model). • Model and measured data errors to be calculated and form part of the uncertainty analysis.
WG4 WP4	Delivery complete.	• Data has been processed. • Use for comparisons against the GH blockage model. • Model and measured data errors to be calculated and form part of the uncertainty analysis.
ReDAPT	Critical path dependency.	• Obtain device power output and inflow data. Compare to GH blockage model and TidalFarmer data binning algorithm for energy prediction. Uncertainty analysis. • Measurement of the site turbulence. Compare to GH flow field, near wake and far wake models. Uncertainty analysis. • Far wake recovery using long range sensor and seabed mounted ADCP. Comparison to GH far wake model. Uncertainty analysis. • Validated CFD model of near wake. Comparison to GH near and far wake models. Uncertainty analysis. • Validation of Tidal Bladed to confirm inflow and Ct,Cp relationship. Provides data to validate how device is modelled. Also, form a comparison with blockage model to predict change in performance characteristics due to operation in depth limited water. • Flow field model results. Comparison to GH flow field model. Uncertainty analysis.

8 REFERENCES

Anderson J.D (1995) *Fundamentals of Aerodynamics*. McGraw-Hill Fourth Edition.

Ainslie, J.F. *Calculating the flowfield in the wake of wind turbines*, Journal of Wind Engineering and Industrial Aerodynamics, 27, 213-224, 1988.

Arango, H.G., and Shchepetkin, A.F. (2012) Regional Ocean Modelling System (ROMS). URL https://www.myroms.org/wiki/index.php/ocean.in.

Blom, P. and Booij, R. Turbulent free-surface flow over sills. Journal of Hydraulic Research, 33, 663–682, 1995.

Bai, L., Spence, R. R. G., Dudziak, G., *Investigation of the influence of array arrangement and spacing on tidal energy converter (TEC) performance using a 3-dimensional CFD model.* Proceedings of the 8th European wave and tidal energy conference, Uppsala, Sweden, 2009.

Blom, P. (1993). *Turbulent Free-Surface Flow Over a Sill*. Ph.D. thesis, Technical University of Delft, Delft, Netherlands.

Bravo, H. R., and Zheng, Y. H. (2000) *Turbulent flow over step with rounded edges experimental and numerical study*. Journal of Hydraulic Engineering, 83-85.

Burton, N., Jenkins, N., Sharpe, D., and Bossanyi, E. (2011) *Wind Energy Handbook*, 2nd edition, John Wiley & Sons.

Buvat, C., Peyrard, C., Menon, J.-M., and Fil, C. (2010a) *Construction of the scale model of a horizontal-axis turbine device and installation of the experimental test platform WG4 WP1 D2*. EDF ETI marine programme project.

Buvat, C. (2010b) *Calibration of tests without turbine WG4 WP1 D3*. EDF ETI marine programme project.

Buvat, C. (2012) *Performance of tank tests with physical scale model of horizontal-axis turbine device installed. Analysis of results WG4 WP1 D4,* ETI Marine programme project.

Chanson, H. (2004) *The hydraulics of open channel flow: An introduction.* Elsevier Butterworth-Heinemann.

Duckworth, A., and Barthelmie, R. J. (2008) *Investigation and validation of wind turbine wake models*. Wind engineering, 32, 5, 459-475.

Durski, S.M., Glenn, S.M., and Haidvogel D. B. (2004) *Vertical mixing schemes in the coastal ocean: Comparison of the leve l 2.5 Mellor-Yamada scheme with an enhanced version of the K profile parameterization.* Journal of Geophysical Research, 109.

Dyer, K. R. and Soulsby, R. L. (1988). *Sand transport on the continental shelf.* Annual Review of Fluid Mechanics, 20, 295–324.

Garrett, C. And Cummins, P. (2005) *The power potential of tidal currents in channels.* Proceedings of the Royal Society, 461, 2563-2572.

Giles, J., Myers, L., Bahaj, A., O'Nians, J., Shelmerdine, B. (2011) *Foundation-based flow acceleration structures for marine current energy converters, IET renewable power generation*, 5, 4, 287-298.

Gretton, G. I. (2011) *Development of a computational fluid dynamics model for an open-centre tidal current turbine WG3 WP5 D2*, ETI Marine programme project.

Gunn, K., and Stock-Williams, C. (2012) *Falls of Warness 3D Model Validation Report*, ETI ReDAPT project.

Jackson, P. S. and Hunt, J. C. R. *Turbulent wind flow over a low hill*. Quarterly Journal of the Royal Meteorological Society, 101, 929–955, (1975).

MacKay, D. (2008) *Sustainable Energy: Without the Hot Air*, www.withouthotair.com, UIT.

Martin, V., Pham, C. T., and Saviot, S. (2012) *Tidal basin modelling: The Alderney Race, the Pentland Firth and the Paimpol-Bréhat sites modelled in Telemac software*, ETI Marine programme project.

McIntosh, S. C., Fleming C. F., and Willden, R. H. J. (2011) Performance and wake structure of a model horizontal axis axial flow turbine. ETI Marine programme project.

Myers, L., Bahaj, A. S., Rawlinson-Smith, R. S., Thomson, M. (2008) *The effect of boundary proximity upon the wake structure of horizontal axis marine current turbines*. In Proceedings of the 27th International Conference on Offshore Mechanics and Arctic Engineering, Estoril, Portugal.

Paterson, A. R. (1983) *A first course in fluid dynamics*. Cambridge University press.

Pope, S. B. (2010) *Turbulent flows.* Cambridge University press.

Salmon, R. (1998) *Lectures on Geophysical Fluid Dynamics*. Oxford University Press.

Schlichting, H., Gersten, K,. (2000) *Boundary layer theory*, Springer-Verlag Berlin.

Song, Y., and Haidvogel, D. (1994) *A semi-implicit ocean circulation model using a generalized topography-following coordinate system*. Journal of Computational Physics, 115, 228-244.

Stallard, T. (2012) *Design and specification of ducted disc experiments WG4 WP3 D1*, ETI Marine programme project.

Tennekes, H., and Lumley, J. L. (1972) *A first course in turbulence*, MIT Press.

Thomson, M.D., and McCowen, D. (2010a) *GH Blockage modelling report WG3 WP4 D1*, GL Garrad Hassan. ETI Marine programme project.

Thomson, M.D., Gill, L., and Collings, R. (2010b) *Near wake modelling report WG3 WP4 D2*, GL Garrad Hassan. ETI Marine programme project.

Thomson, M.D., Whelan, J.I. (2010c) *Device scale modelling report WG3 WP4 D3*, GL Garrad Hassan. ETI Marine programme project.

Thomson, M.D., Collings. R., and Stallard, T. (2011a) *Array scale experimental test report WG4 WP2 D5*, GL Garrad Hassan. ETI Marine programme project.

Thomson, M. D. And Gill, L. (2011b) *Rationalised flow field modelling report WG3 WP4 D4*, GL Garrad Hassan. ETI Marine programme project.

Thomson, M.D., Gill, L., and Collings, R. (2011c) *Far wake modelling report WG3 WP4 D5*, GL Garrad Hassan. ETI Marine programme project.

Trefethen, L. N. (2000). *Spectral Methods in Matlab*. Society for Industrial Mathematics.

Vermeer, L. J., Sorenson, J. N., Crespo, A. (2003) *Wind turbine wake aerodynamics*. Progress in Aerospace Sciences, 39, 467-510, 2003.

Weideman, J. A. C. and Reddy, S. C. (2000). *A MATLAB differentiation matrix suite*. ACM transactions on mathematical software, **26**, 465–519.

Whelan, J. I., Graham, J. M. R., and Piero, J. (2009) *A free-surface blockage correction for itdal turbines in an array*. Journal of Fluid Mechanics. 624, 281-291.

Wickham, A., and Way, S. P. (2012) *Construction, calibration, testing and reporting of coastal basin scale experiments.* GL Garrad Hassan. ETI Marine programme project.

Wood, R. M. and Harris, R. G. (1920), *Some notes on the theory of an airscrew working in a wind channel*, Reports & Memoranda No. 662, Aeronautical Research Committee.

9 APPENDIX A: EXPERIMENT SUMMARY

Table 9: Summary of different studies that will be used to validate the GH blockage, far wake and near wake models.

Test	Institute	Scale	Type	Turbulence intensity (%)	Inflow speed (m/s)	Rotor/Disk Diamater (m)	Channel width (m)	Channel depth (m)	Area blockage (%)	Vertical blockage	Lateral blockage	Blockage model	Near wake	Far wake
A	WG3 WP1	1:1	Rotor	-	2.1	18	72	36	10%	50 %	25 %	Y	Y	Y
B	WG3 WP1	1:1	Rotor	-	2.1	18	27	36	52%	50 %	66 %	Y	Y	
01	WG4 WP1	1:30	Rotor	5-8	0.27	0.6	1.5	0.8	24 %	75 %	40 %	Y	Y	Y
02	WG4 WP1	1:30	Rotor	15	0.27	0.6	1.5	0.8	24 %	75 %	40 %	Y	Y	
03	WG4 WP1	1:30	Rotor	5-8	0.55	0.6	1.5	0.8	24 %	75 %	40 %	Y	Y	
04	WG4 WP1	1:30	Rotor	5-8	0.27	0.6	1.5	1.0	18 %	60 %	40 %	Y	Y	
05	WG4 WP1	1:30	Rotor			0.6	1.5	0.8	24 %	75 %	40 %	Y	Y	
05	WG4 WP2	1:70	Rotor	8-10	0.50	0.27	5	0.45	2 %	60 %	5 %	Y	Y	Y
06	WG4 WP2	1:70	Rotor	8-10	0.50	0.27	5	0.45	5 %	60 %	13 %	Y	Y	Y
07	WG4 WP2	1:70	Rotor	8-10	0.50	0.27	5	0.45	5 %	60 %	16 %	Y	Y	Y
08	WG4 WP2	1:70	Rotor	8-10	0.50	0.27	5	0.45	5 %	60 %	21 %	Y	Y	Y
09	WG4 WP2	1:70	Rotor	8-10	0.50	0.27	5	0.45	8 %	60 %	21 %	Y	Y	Y
10	WG4 WP2	1:70	Rotor	8-10	0.50	0.27	5	0.45	8 %	60 %	27 %	Y	Y	Y
11	WG4 WP2	1:70	Rotor	8-10	0.50	0.27	5	0.45	8 %	60 %	37 %	Y	Y	Y
12	WG4 WP2	1:70	Rotor	8-10	0.50	0.27	5	0.45	8 %	60 %	21 %	Y	Y	Y
19	WG4 WP2	1:70	Rotor	8-10	0.50	0.27	5	0.45	2 %	60 %	5 %	Y	Y	Y
26a	WG4 WP2	1:70	Rotor	8-10	0.50	0.27	5	0.45	8 %	60 %	21 %	Y	Y	Y
TBC	WG4 WP3	1:70	Ducted	TBC	TBC	0.27	1.5	TBC	TBC	TBC	TBC	Y		Y
2	WG4 WP4	1:300	Actuator	10-20	0-0.70	0.11	9.0	0.2	7 %	55 %	20 %	Y		
4	WG4 WP4	1:300	Actuator	10-20	0-0.70	0.11	9.0	0.2	21 %	55 %	58 %	Y		